Environmental Earth Sciences (2021) 80:51
https://doi.org/10.1007/s12665-020-09281-z

ORIGINAL ARTICLE

Hydrochemical and environmental isotope characteristics of groundwater in the Hongjiannao Lake Basin, Northwestern China

Wenping Mu[1] · Xiong Wu[2] · Chu Wu[2] · Qian Hao[2] · Ruochen Deng[2] · Cheng Qian[3]

Received: 9 July 2019 / Accepted: 16 November 2020 / Published online: 11 January 2021

Abstract

Understanding the hydrochemical and isotopic characteristics of groundwater and hydrogeochemical processes is crucial for groundwater resource development and environmental protection, especially in semiarid regions. To address this question, we collected and tested groundwater and river water samples form the Hongjiannao Lake Basin. The groundwater samples were took from a porous medium aquifer and a pore-fissure aquifer. We studied hydrochemical characteristics of groundwater from both aquifers using major element measurements, statistical calculations, and the use of Piper diagrams. The hydrogeochemical processes taking place in groundwater were identified using the Gibbs diagram, Gaillardet diagram, saturation index calculations, ratios of major ions, and chloro-alkaline indices. We also investigated the origin of groundwater using stable isotopes (D and ^{18}O) and evaluated groundwater age on the basis of piston model of tritium isotope (^{3}H) measurements. Groundwater–river water interactions are also identified using chemical and stable isotope characteristics. The results show that groundwater in both aquifers has a chemical composition dominated by are HCO_3 anions that groundwater has a low total dissolved solids (TDS) content. An assessment of the analyzed groundwater chemical data suggests that feldspar dissolution, the dissolution/precipitation of carbonate minerals (dolomite and calcite), and cation exchange play an important role in the hydrochemical evolution of groundwater in the study area. The compositions of stable isotopes and tritium imply that groundwater in the porous medium and pore-fissure aquifers originate from modern and ancient precipitation sources, respectively. The groundwater recharge is influenced by evaporation as water infiltrates through the vadose zone. In addition, river, lake, and groundwater form an organic whole. This study provides effective guidance for groundwater resource development and environmental protection in a similar area.

Keywords Groundwater · Hydrochemical characteristics · Hydrogeochemical processes · Isotopic characteristics · Semiarid region

Introduction

Groundwater plays a significant role in domestic water, agricultural irrigation, and industrial production in semiarid and arid areas around the world because of the scarcity and/or poor quality of surface water (Adams et al. 2001; Taylor et al. 2012; Houatmia et al. 2016; Wang et al. 2017b). Groundwater is commonly the primary recharge source of inland lakes, which are an important component of wetland systems (Winter et al. 1999; Hou et al. 2008a, b; Zhao et al. 2008; Su et al. 2016), provides water for vegetation (Gribovszki et al. 2010; Yin et al. 2011a), and is therefore, a key factor to maintain ecosystem stability (Su et al. 2016). The hydrochemical evolution and circulation features of groundwater are crucial issues for sustainable groundwater resource use and environment protection. However, traditional hydrogeology surveys are insufficient to completely address these questions (Yin et al. 2011b; Wang et al. 2017b). Studies into the hydrochemical and isotopic characteristics of groundwater and hydrogeochemical processes are, therefore, required.

The chemistry and isotopic composition of groundwater carries important information that functions as a chemical

✉ Xiong Wu
wuxiong@cugb.edu.cn

[1] School of Engineering and Technology, China University of Geosciences (Beijing), Beijing 100083, China

[2] School of Water Resources and Environment, China University of Geosciences (Beijing), Beijing 100083, China

[3] Construction Engineering Quality and Safety Supervision Station, Housing and Construction Bureau of Dapeng New District, Shenzhen 518119, China

fingerprint for provenance. Chemical analysis can be used to unravel the formation and evolution of groundwater components. Environmental isotope data (e.g., D, ^{18}O, ^{3}H) can further deepen the understanding of groundwater circulation (Yang et al. 2004, 2009, 2018b; Hu et al. 2014; Wang et al. 2017b). The hydraulic connection between groundwater and surface water can also be identified through a comparison of chemical and isotopic compositions (Su et al. 2009; Yang et al. 2016, 2018b).

Statistical calculations, correlation analysis, and Piper diagrams are widely used to investigate hydrogeochemical characteristics, whereas hydrogeochemical diagrams (e.g., Gibbs, Gaillardet) (Li et al. 2015; Wang et al. 2017b), solubility equilibrium (Qian et al. 2016), and chloro-alkaline indices are often employed to infer hydrogeochemical processes (Yang et al. 2016, 2018a). Hydrogeochemical components change along the groundwater flow direction, which is determined by the dominant hydrogeochemical process (e.g., mineral dissolution or precipitation, ion exchange, mixing effects) (Li et al. 2015; Wang et al. 2017b; Yang et al. 2018a). The origin of groundwater is identified by stable isotopes, D and ^{18}O, as widely reported in the literature (Katz et al. 2010; Yin et al. 2011b; Hu et al. 2014; Yang et al. 2018a, b). The tritium isotope (^{3}H) composition can be used to estimate the age and renewability of groundwater (Yang et al. 2004; Qin et al. 2011; Cartwright and Morgenstern 2012; Zhao et al. 2014).

To demonstrate these principles, we selected the Hongjiannao Lake Basin as a case study. The basin is located in the northeastern part of the Ordos Basin in northwestern China, and possesses not only rich mineral resources (e.g., coal, natural gas, oil) but is also an ecologically vulnerable area (Hou et al. 2008a, b; Yin et al. 2010). Many investigations have been conducted in the the northeastern part of the Ordos Basin at the regional (i.e., basin) scale to meet groundwater resource demands for basic energy construction and environmental protection. These studies have involved the division and characteristics of the groundwater system (Hou et al. 2007, 2008a, b), chemical and isotopic characteristics (Li et al. 2006; Yang et al. 2009), groundwater origin and circulation (Zhao et al. 2008; Yin et al. 2010), potential groundwater development (Wang et al. 2002; Hou et al. 2017), and pollution analysis (An and Lu 2018). In general, the groundwater quality was comparatively good in this region. The hydrochemical type is mainly HCO_3 type with total dissolved solids (TDS) of less than 1.0 g/L (Li et al. 2006). The composition of hydrogen and oxygen isotopes indicates that groundwater is derived from the atmospheric precipitation (Hou et al. 2008a, b). The slope of local meteoric water line (LMWL) is less than the slope of the global meteoric water line (GMWL) because of the semiarid climate characteristics of the region (Yin et al.2011b).

Some large lakes, such as the Hongjiannao Lake or Subei Lake located north of the Ordos Basin, are the discharge area of the local groundwater system, which plays an important role for sustaining these ecosystems (Liu et al. 2015). However, few studies have reported on the hydrogeochemical processes and circulation characteristics of groundwater in the lake basin at the local scale (Yin et al. 2011a; Li et al. 2013b). Meanwhile, information regarding the interaction of groundwater with surface water bodies at the local scale remains scarce (Qian et al. 2016). Further investigation is, therefore, essential for groundwater resource development and environmental protection.

In the present study, we use hydrochemistry and environmental isotopes (D, ^{18}O, ^{3}H) to address two questions: (1) the identification of groundwater hydrochemical characteristics and of hydrogeochemical processes; (2) the determination of environmental isotope characteristics and thus the origin and age of the groundwater. We have used the Hongjiannao Basin, a subsystem of a larger regional groundwater system, as a case study.

Study area

Physical geography

The study area is about 50 km from the city of Ordos in the northeastern part of the Ordos Basin (Fig. 1). The study area perimeter was identified according to hydrological analysis using ArcGIS software and encompasses with an area of about 1400 km^2. The study area lies in a semiarid region and rainfall is concentrated from June to September with a long-term average rainfall of about 380 mm/yr. The long-term average potential evaporation rate is approximately 2000 mm/yr and the average annual temperature is 8.9 °C.

Hongjiannao Lake is located in the eastern part of study area and is a wetland of national ecological significance (Fig. 1). The lake area is about 40 km^2 with an average depth of 5 m. The hydrochemical type of the lake water is Na-Cl. The pH is 9.7 and electrical conductivity is 11.3 mS/cm. The TDS is about 7.0 g/L, which is indicative of a saline lake. There are five perennial rivers that drain into the lake; the most important of which are the Zhashake River, the Manggaitu River, and the Qipusu River (Fig. 1). The length of these rivers is less than 30 km and their discharge rates are generally less than 0.5 m^3/s. The topography is relatively flat with a surface elevation of 1200–1550 m, high on all the sides, and low around the Hongjiannao Lake area (Fig. 1). The geomorphology is dominated by rolling plateaus and the ground surface is covered by fine Holocene sand (Figs. 2, 3).

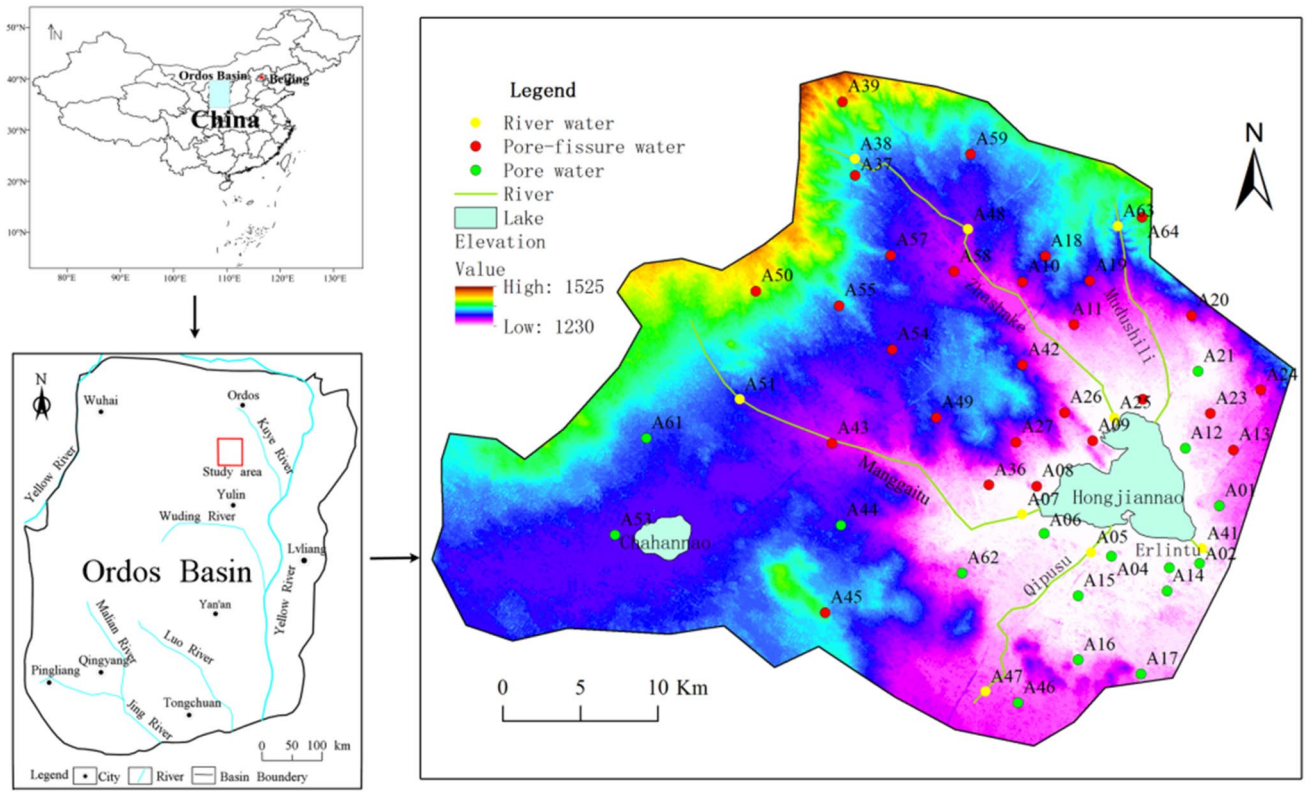

Fig. 1 Location, sample points, and ground elevation of the study area (color figure online)

Geological and hydrogeological setting

The study area is within a west-striking monoclinal structure with a dip angle of 1° to 2° and few developed faults (Hou et al. 2007; Jiang et al. 2018) (Figs. 2, 3). The main strata include Jurassic clasolite, Cretaceous clasolite, and loose Quaternary sediments, which are further divided into Upper Pleistocene and Holocene strata (Fig. 3). The Cretaceous clasolite is practically covered by the Holocene stratum in the northern section and is covered by Upper Pleistocene and Holocene strata in the southwestern and southeastern sections (Figs. 2, 3). The mineralogy of the Cretaceous clasolite (Hou et al. 2008a, b; Xie et al. 2012; Qian et al. 2016) and Upper Pleistocene stratum (Li et al. 1991; Qian et al. 2016) include feldspar, dolomite, calcite, gypsum, and a small amount of soluble salt.

A Quaternary porous medium aquifer and Cretaceous pore-fissure aquifer are the major aquifers in the study area and are both unconfined. The porous medium aquifer is underlies in the southwestern and southeastern sections of the study area and is mainly composed of Pleistocene fluvial–lacustrine sediments with low clay content, which consist of unconsolidated medium sands, fine sands, and silty sands with clayey-sand lenses (Wu et al. 2018). The thickness of the porous medium aquifer ranges from 0 to 30 m with an average of approximately 20 m. The depth of the groundwater level ranges from 0.7 to 4.6 m with an average of approximately 2.3 m. The hydraulic conductivity ranges from 3.9 to 11.0 m/d and the specific well discharge ranges from 0.4 to 1.5 L/(s·m) (Wu et al. 2018). In general, the water yield property is relatively promising with regards to the specific well discharge.

The pore-fissure aquifer is widely distributed and can be regarded as large-scale homogeneous aquifer (Jiang et al. 2018). It is mainly composed of early Cretaceous riverine and aeolian sediments (Hou et al. 2008a, b) and its lithology is dominated by gritstone, medium sandstone, and fine sandstone with mudstone lenses, which are characterized by poor cementation, good connectivity, coarse particles, high porosity, and a complex sedimentary rhythm (Xie et al. 2005; Deng et al. 2008; Hou et al. 2008a, b; Qian et al. 2016). These characteristics control the permeability and water yield properties. In general, the aquifer thickness decreases from west to east and ranges up to 450 m with an average of approximately 240 m. The depth of the groundwater level decreases from west to east in the aquifer and ranges from 2 to 80 m with an average of approximately 15 m. The hydraulic conductivity ranges from 0.4 to 1.5 m/d with an average of approximately 0.6 m/d (Hou

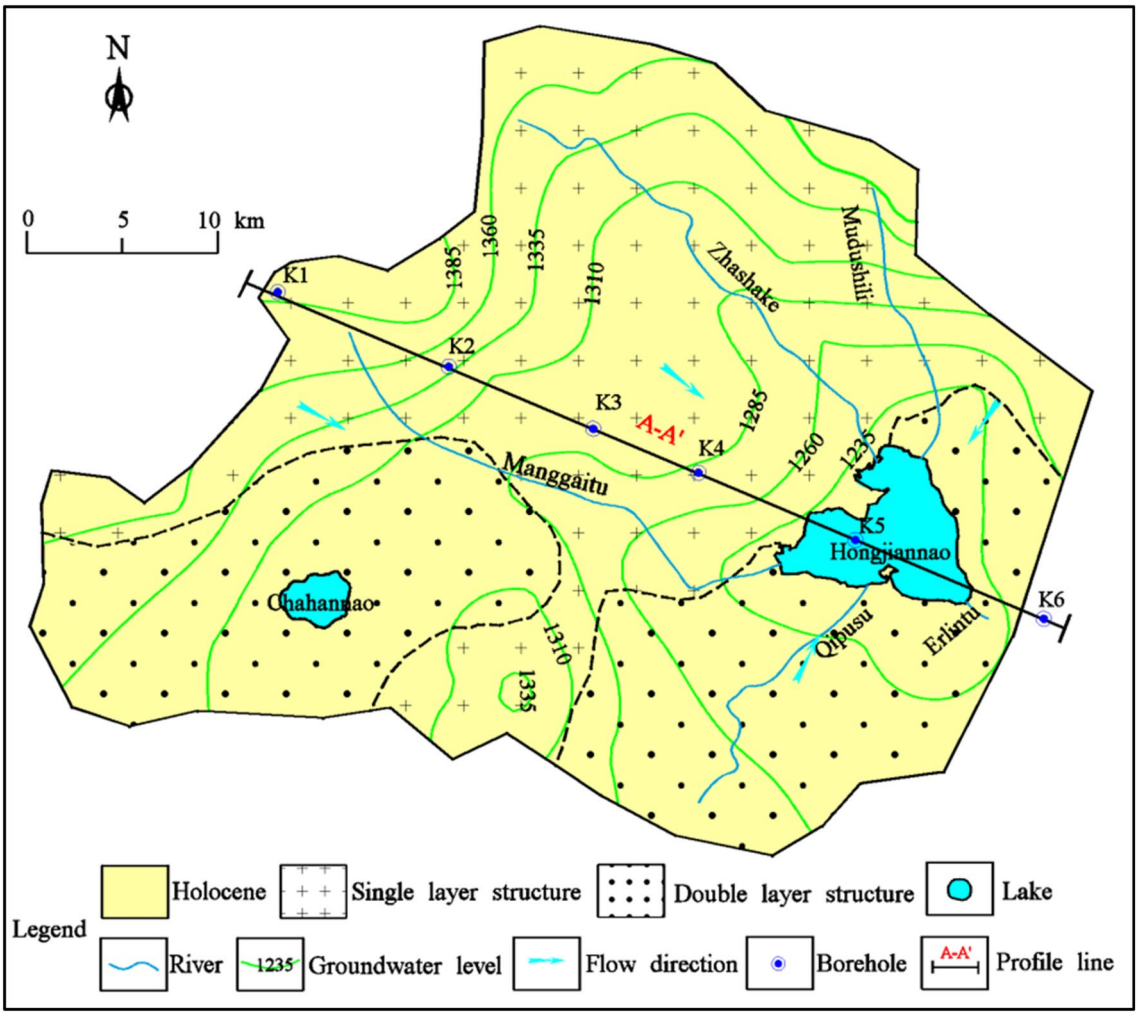

Fig. 2 Hydrogeological map of the study area (color figure online)

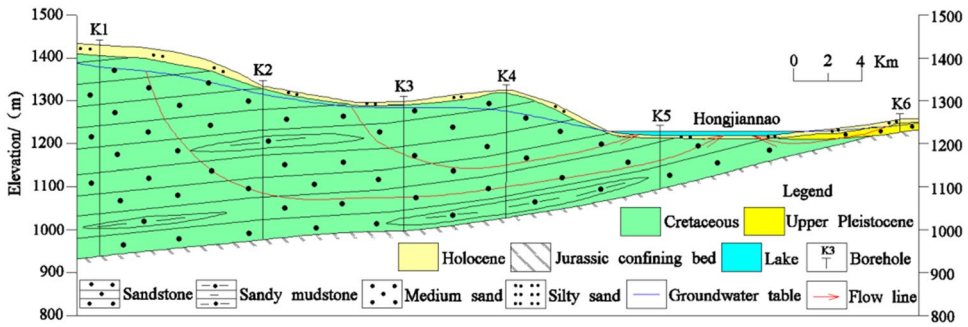

Fig. 3 A-A' hydrogeological profile in Fig. 2 (color figure online)

et al. 2008a, b). The specific well discharge ranges from 0.13 to 0.21 L/(s·m) and the water resources are abundant.

The Jurassic clasolite underlying the pore-fissure aquifer is composed of interbedded sandstone and sandy mudstone with good consolidation and poor permeability (Hou et al. 2007, 2008a, b) and is therefore regarded as the lower confining bed (Fig. 3). On the basis of the above analyses, the groundwater system structure is divided into two types: (1) a double-layer structure consisting of the porous medium aquifer and pore-fissure aquifer and (2) a single layer structure consisting of the pore-fissure aquifer. There is a close hydraulic connection between the porous medium aquifer and pore-fissure aquifer in the double-layer structure area because a continuous aquiclude is not present (Figs. 2, 3).

These two aquifers, therefore, form a unified groundwater flow system (Hou et al. 2007, 2017).

According to a field investigation in August 2018, freshwater resources are stored in the porous medium and pore-fissure aquifers. In general, groundwater from all directions flows into Hongjiannao Lake (Figs. 2, 3). The lake drainage is mostly responsible for groundwater discharge and exploitation for agriculture irrigation and domestic water supply is secondary (Hou et al. 2007; Zhao et al. 2008). The groundwater furthermore maintains the local ecosystem stability.

Materials and methods

Sample collection and testing

Fifty-one representative groundwater ($n=43$) and river water ($n=9$) sampling points were selected in August 2018. The rainfall of the period is abundant each year, which is called as the high-water period in below. The same sampling points were selected in March 2019. The rainfall of the period is scarce each year, which is called as the low-water period in below (Fig. 1). Among the groundwater sampling points, 16 were selected for sampling the porous medium aquifer, and 27 were selected for sampling the pore-fissure aquifer (Fig. 1). The concentrations of major ions and other chemical constituents were chemically analyzed in each water sample (Tables 1, 2).

All sampling points were chosen to measure the stable isotope (D, ^{18}O) in the high-water period. Among these, 8 porous medium aquifer and 13 pore-fissure aquifer sampling points were chosen to measure tritium (^{3}H) in the high-water period (Table 1). All samples were stored in polyethylene bottles and the bottle mouth was closed using parafilm.

Samples were analyzed in the Analytical Laboratory Beijing Research Institute of Uranium Geology for major cations (K^+, Na^+, Ca^{2+}, Mg^{2+}), major anions (HCO_3^-, CO_3^{2-}, SO_4^{2-}, Cl^-, NO_3^-), TDS, stable isotopes (D and ^{18}O) and tritium (^{3}H) (Tables 1, 2). Among these parameters, Ca^{2+}, Mg^{2+}, Na^+, K^+, SO_4^{2-}, and Cl^- were determined using ion chromatography and CO_3^{2-} and HCO_3^- were analyzed with titrimetric methods. Stable isotopes of D and ^{18}O were determined using a gas isotope mass spectrograph and ^{3}H was tested using a low-background liquid scintillation counter. The pH, electrical conductivity, and temperature were also obtained using a HANNA test pen in the field (Tables 1, 2).

Isotope ratios are expressed in terms of deviation from the Vienna Standard Average Ocean Water (VSMOW):

$$\delta(\%) = \frac{R_{Sample} - R_{VSMOW}}{R_{VSMOW}} \times 1000, \quad (1)$$

where δ is the isotopic deviation in %, R_{Sample} is the isotope ratio (D/H or $^{18}O/^{16}O$) in the sample, and R_{VSMOW} is the isotope ratio in VSMOW.

Chemical data assessment methods

A number of standard graphical and numerical techniques were used to assess in the chemical data provided in Tables 1, 2 to determine the physical and chemical processes that are most likely to be influencing the chemical composition of groundwater in the study area.

The first of these techniques was the use of a Gibbs diagram. This uses includes the relationship between mass ratio $Na^+/(Na^+ + Ca^{2+})$ and TDS and the relationship between mass ratio $Cl^-/(Cl^- + HCO_3^-)$ and TDS (Gibbs et al. 1970). The diagram is widely used to estimate the origin of hydrochemical components in natural water (Li et al. 2013b; Wang et al. 2017a, b). There are three endmembers in the diagram: precipitation dominance; water–rock interaction dominance; and evaporation dominance (Gibbs et al. 1970; Wang et al. 2015). A Gaillardet diagram was used to further determine water–rock interaction types and also has three endmembers determined by stratum mineralogy (Gaillardet et al 1997, 1999; Singh et al. 2012): calcite and dolomite dissolution; feldspar dissolution; and evaporite dissolution.

The ratio of major components can reveal hydrogeochemical processes that control the chemistry because of their interrelation in groundwater (Hussein 2004; Yang et al. 2018a, b). The saturation index (*SI*) is also widely used to analyze whether specific minerals are likely to be precipitating or dissolving in aquifer sediments. The ratio of major ions and *SI* are, therefore, used to verify and supplement the information regarding the types of water–rock interaction. The *SI* is defined as:

$$SI = \lg\left(\frac{IAP}{K_S(T)}\right), \quad (2)$$

where *IAP* is the ion activity product of dissolution and K_S (T) is the dimensionless solubility product constant of a mineral considered at temperature T (°C).

A mineral in solution is unsaturated if the *SI* value is less than zero. *SI* is exactly equal to zero when the mineral in solution reaches equilibrium between saturation and precipitation. A positive *SI* value suggests that the mineral in solution is over saturated. The PHREEQC software (version 2.8) was used to calculate *SI* values in this study.

The chloro-alkaline indices *CAI*-1 and *CAI*-2 can be used to determine the occurrence of cation exchange (Li et al. 2013a, b; Houatmia et al. 2016; Yang et al. 2018a, b). For example, Ca^{2+} in groundwater exchanges with Na^+ in the aquifer media. If the *CAI*-1 and *CAI*-2 are both

Table 1 Hydrochemistry and environmental isotope test results in the high-water period

Types	Samples	pH	Temp ℃	EC mS/cm	Cl^-	SO_4^{2-} mg/L	HCO_3^-	CO_3^{2-}	Na^+	K^+	Mg^{2+}	Ca^{2+}	NO_3^-	TDS	δD (%)	$\delta^{18}O$	^3H (TU)
Pore water	A01	8.47	15.8	0.72	12.5	78.9	270	0	32.9	1.31	14.8	88	37.0	400	− 61.3	− 7.2	10.6
	A02	8.57	18.2	0.57	13.8	35.2	241	0	12.8	1.99	19.7	68.1	16.6	289	− 58	− 7	–
	A03	8.19	13.0	0.53	13.9	31.3	247	0	16.7	2.42	14.1	63.3	0.46	266	− 62.8	− 7.5	15.1
	A04	8.02	14.1	0.39	4.98	23.5	182	0	10.1	1.55	10.1	49.3	3.71	194	− 57.7	− 7.7	–
	A06	7.66	14.3	1.21	41.7	228.0	323	0	59.6	1.91	23.5	147	11	674	− 64.1	− 6.9	11.8
	A12	7.63	15.3	0.68	9.85	62.7	277	0	24.2	0.76	13.1	89.5	26.2	365	− 71	− 8.8	4.7
	A14	8.51	12.5	0.44	5.16	20.5	216	0	10.4	1.24	11.0	56.2	0	213	− 58	− 7.9	17.7
	A15	7.66	19.2	1.06	46.6	55.4	481	0	64.2	9.73	40.0	87.7	2.12	546	− 62.3	− 8.2	–
	A16	7.79	11.1	0.46	7.43	18	206	0	16.5	0.96	10.7	54	16	227	− 67.8	− 8.8	–
	A17	7.51	14.2	0.56	7.56	21.2	301	0	19.8	1.12	13.2	74.7	1.56	290	− 64	− 8.6	18.5
	A21	7.82	13.3	1.19	89.1	112	301	0	152	0.95	11.4	67.1	48.4	631	− 80.6	− 10.6	–
	A44	8.11	13.6	1.06	104	102	330	0	39.5	1.8	27.6	119	1.02	560	− 67.5	− 8.3	–
	A46	7.7	12.0	0.57	15.9	49.2	254	0	19.2	2.45	15.9	69.5	0.34	299	− 62.9	− 8.3	13.4
	A53	8.5	16.0	0.47	15.8	8.03	218	0	16.1	5.21	13.4	43.1	3.9	215	− 59.6	− 7.4	–
	A61	7.61	15.9	0.49	6.82	38.6	241	0	13	1.24	14.7	63.7	0	259	− 60.3	− 7.3	20.1
	A62	8.03	12.8	0.47	8.0	31.7	221	0	16.7	1.48	11.1	58.3	1.45	239	− 66.2	− 8	–
Pore– fissure water	A08	8.68	13.2	0.60	28.1	36	220	0	95.5	0.78	5.25	18.2	21.9	316	− 72	− 8.5	4.9
	A09	8.26	14.2	0.67	29.1	47.1	261	0	122	0.72	5.45	10.5	10.7	356	− 78.1	− 9.2	–
	A10	8.37	13.1	0.42	9.56	30.2	187	0	22.5	1.4	16.7	41.2	21.5	237	− 61.4	− 8.2	5.3
	A11	8.64	21.1	0.64	32.4	38	227	0	92.3	0.68	5.09	15.3	28.3	326	− 72.6	− 9.2	2.8
	A13	7.82	13.7	0.50	9.49	19.9	234	0	15.2	1.97	15.4	35	13.6	228	− 66.4	− 8.1	–
	A18	7.74	13.2	0.49	7.62	26.3	214	0	12.3	0.93	10.7	67.2	28.2	260	− 61.7	− 8.2	–
	A19	7.91	14.1	0.41	6.5	18	190	0	59	0.48	3.61	18.4	11.2	212	− 73.5	− 9.2	< 1.3
	A20	8.21	12.8	0.42	5.08	14.3	192	0	34.3	0.57	9.47	36	28.5	224	− 62.8	− 6.6	–
	A22	8.66	13.0	0.82	37.6	55.5	294	0	131	1.04	9.04	21.8	15.6	419	− 76	− 9.3	< 1.3

Table 1 (continued)

Types	Samples	pH	Temp ℃	EC mS/cm	Cl^-	SO_4^{2-} mg/L	HCO_3^-	CO_3^{2-}	Na^+	K^+	Mg^{2+}	Ca^{2+}	NO_3^-	TDS	δD (%)	$\delta^{18}O$	^3H (TU)
Pore– fissure water	A23	7.87	14.2	1.02	59.4	58.4	271	0	35.9	2.42	34.3	95.2	95.4	517	– 66.4	– 8.6	–
	A24	7.81	13.4	1.07	79.1	38.2	333	0	92.9	1.1	29	58.3	59.7	525	– 68.1	– 9	2.0
	A26	7.93	14.8	0.71	21.1	30.6	247	0	55.9	0.59	15.7	55.4	77.8	381	– 71.5	– 8.6	–
	A27	7.97	13.1	0.41	7.88	14.6	183	0	38.3	0.61	8.63	29.8	18.3	210	– 72.8	– 9.8	< 1.3
	A36	9.62	13.1	0.70	33.1	58.1	202	14.6	138	0.75	0.72	3.37	16.5	366	– 79.4	– 9.3	< 1.3
	A37	8.02	13.5	0.59	18.6	22	231	0	22.7	0.84	21.9	56.4	48.5	306	– 61.6	– 7.8	–
	A39	8.08	14.1	0.50	11.7	14.3	224	0	13.3	1.17	20.8	49.2	24.9	247	– 69.7	– 9.1	< 1.3
	A42	7.78	11.9	0.51	6.57	25.6	234	0	12.7	0.76	11	48.8	19.9	242	– 63.7	– 7.9	–
	A43	9.61	13.9	0.67	50.8	93.8	198	11	132	0.38	1.18	2.51	8.57	399	– 79.8	– 9.4	< 1.3
	A45	7.97	13.6	0.53	16.1	15.6	187	0	13.2	1.4	14.1	63.9	71.9	290	– 68.4	– 9.3	< 1.3
	A49	8.33	12.7	0.56	15.1	24.1	209	0	16	1.25	12.9	67.9	48	290	– 64.4	– 8.8	–
	A50	8.07	13.5	0.46	5.74	8.02	226	0	24	0.78	17.4	40.2	24.9	234	– 70.4	– 9	–
	A54	7.79	15.2	0.72	19.7	71.6	300	0	42	4.38	32.1	49.9	5.8	375	– 60.7	– 7.2	–
	A55	7.53	14.1	0.76	36.9	22	284	0	22.6	1.13	24.5	82.8	63.9	396	– 66.2	– 7.2	< 1.3
	A57	8.66	13.7	0.65	22.1	27	224	0	37.8	0.87	24.6	44.3	58.2	327	– 63.6	– 7.6	–
	A58	8.25	12.8	0.79	22.5	48.8	351	0	115	0.75	14.3	27	4.64	408	– 71.3	– 7.6	–
	A59	7.62	12.3	0.67	15.6	35.5	321	0	19.3	0.52	17.9	88	13	350	– 63.4	– 8.3	–
	A64	8.07	11.8	0.45	10.8	11.4	185	0	11.4	0.40	15.4	49.7	37	229	– 65.2	– 8.2	2.2
River water	A05	8.86	27.7	0.66	27.8	46.7	296	0	54.8	5.23	22.5	46.7	0.83	353	– 60.6	– 7.1	–
	A07	8.65	30.7	1.51	66.2	287	364	0	248	4.62	23.6	33	2.99	847	– 64.6	– 8.4	–
	A25	8.6	31.9	0.72	41.6	54	298	0	80.7	1.89	23.8	36.7	0.26	388	– 50.6	– 6.4	–
	A38	8.55	29.3	0.49	10.9	6.26	252	6.29	24.2	1.33	21.6	40.1	0.69	237	– 59.5	– 7.6	–
	A41	8.42	21.5	1.30	82.6	47.7	573	0	223	3.64	20.5	28.8	4.02	697	– 48	– 6.7	–
	A47	8.2	18.5	0.48	9.92	22.6	236	0	22.1	2.31	11.7	54.4	20	261	– 62.3	– 8.2	–
(%)River water	A48	7.98	19.4	0.86	30.3	43.2	374	0	48.4	2.44	32.9	69.5	15.9	430	– 62.3	– 7.8	–
	A51	8.45	31	0.72	41.8	14.2	327	12.3	68.5	2.04	32.3	39.1	0.413	374	– 51.1	– 6.4	–
	A63	8.45	20.7	0.55	7.82	7.74	298	0	18.8	0.93	16.2	63.5	1.52	266	– 58.8	– 7.8	–

Temp is the abbreviation for temperature, '–' represents samples that were not tested

Table 2 Hydrochemistry and environmental isotope test results in the low-water period

Types	Samples	pH	Temp ℃	EC mS/cm	Cl^- mg/L	SO_4^{2-}	HCO_3^-	CO_3^{2-}	Na^+	K^+	Mg^{2+}	Ca^{2+}	NO_3^-	TDS
Pore water	A01	7.67	11.5	0.8	16.7	94.8	93.5	0	33.8	1.1	15.6	42.8	63.6	315
	A02	8.12	15.5	0.53	15.7	48.4	129	0	15.4	2.04	16.8	35	9.59	207
	A03	8.05	11.8	0.66	20.7	40.5	203	0	23.1	2.5	16.5	44.2	0.75	250
	A04	8.34	11	0.41	5.1	29.3	142	0	9.94	1.37	10.7	37.4	1.43	166
	A06	8.01	10.1	1.21	43.3	255	204	0	58.4	1.7	27.4	116	16.2	620
	A12	7.57	11.5	0.66	8.3	51.9	220	10	18.5	0.59	13.3	76.7	14.8	294
	A14	8.48	8.6	0.4	5.28	21.2	188	5.39	10.6	1.2	10.7	50.1	< 0.08	193
	A15	8.16	12	0.58	10.9	45.4	209	8.78	18.6	1.06	16.2	62.2	14	273
	A16	8.2	9.4	0.52	6.97	23.2	205	0	16.9	0.85	12.3	50.9	11.84	225
	A17	8.19	10.8	0.57	8.43	23.7	201	0	19.4	1.09	13.6	45.3	0.97	213
	A21	9.09	12.1	0.7	37.3	54.2	221	11	139	0.61	1.3	5.38	16	364
	A44	7.94	10.1	0.77	45	61	155	4.84	25.4	1.43	17.7	54.9	0.33	283
	A46	7.92	11.2	0.74	27	57.3	146	9.76	23.1	2.41	20.1	43.5	0.37	247
	A53	8.32	8.9	0.44	20.9	9.51	180	12.4	15.9	5.75	14.8	45.7	1.1	204
	A61	8.02	8.9	0.49	6.24	37.7	122	7.91	13	1.18	14.7	31.8	0.45	166
	A62	8.55	11.3	0.49	8.3	39.1	114	5.57	14.6	1.61	11.4	32.9	0.39	165
Pore-fissure water	A08	9.15	13.6	0.62	35.2	48.5	197	6.85	121	1.01	2.89	10.7	19.7	338
	A09	8.72	13.5	0.65	27.6	42.2	244	14.1	120	1.15	6.67	13.5	5.07	338
	A10	8.5	10.9	0.44	9.11	27.8	156	8.98	31.6	1.11	14.1	30.9	21	214
	A11	8.02	12.6	0.39	4.67	22.6	177	8.98	54.4	0.56	7.62	16.8	0.62	196
	A13	7.81	12.9	0.48	8.17	20.2	192	8.08	18.3	2.09	16	46.6	14.6	222
	A18	8.38	10.7	0.52	7.94	36.3	109	4.64	12.8	0.9	11	41.7	30.6	196
	A19	8.25	12.8	0.45	7.14	24.8	181	7.46	67.5	0.41	4.65	16.2	10.5	222
	A20	7.93	11.7	0.45	4.1	25.2	182	10.7	66.8	0.64	5.14	18.7	16.7	228
	A22	9.43	12.2	0.87	37.9	94.5	237	13.3	177	0.67	< 0.05	5.12	16	450
Pore–fissure water	A23	7.36	12.8	1.01	61.2	60.8	189	10.3	37.8	2.51	35.3	79	110	481
	A24	7.87	11.9	0.84	59.6	20.5	181	12.2	84.5	1.08	22.3	19.1	42.7	340
	A26	8.19	12	0.46	5.67	28	198	11.6	79.5	0.40	4.72	11.7	6.85	236
	A27	7.7	8.8	0.48	7.68	21	132	9.03	17.2	0.66	11.6	36.6	22.7	183
	A36	7.77	11.1	0.47	31.8	58.9	213	12.3	137	0.96	1.88	6.22	15.9	359
	A37	7.98	10.3	0.68	24	41.5	155	7.73	28.9	0.88	25.3	42.5	70.3	311
	A39	7.95	10	0.49	11.9	16.5	179	6.37	13.1	1.14	21	39.2	25.1	217
	A42	7.77	11.5	0.49	5.71	24.8	114	5.51	12.8	0.77	10.5	33.8	20.7	166
	A43	9.36	11.4	0.63	43.8	42.8	202	9.91	127	0.27	1.66	3.3	7.84	328
	A45	7.58	12.7	0.53	15.6	15.7	93	5.09	13.5	1.29	13.9	37	61.1	205
	A49	9.76	10.9	0.71	9.48	17.4	148	6.96	15.3	1.32	12.1	44.7	44.1	218
	A50	7.9	10.5	0.46	5.36	7.9	172	10.3	24.2	0.75	17.7	30.1	23	195
	A54	7.64	11.5	0.7	15.3	53.2	185	10.1	76.6	1.05	18.2	16.6	32.7	306
	A55	7.97	11.3	0.58	13.6	13.1	144	7.65	21	1.16	21.9	25.7	35.5	204
	A57	8.49	11.2	0.6	22.9	23.9	158	10.6	39.5	0.83	27.1	25.3	58.6	277
	A58	8.14	11.6	0.73	23	43.7	255	18.2	117	0.72	13.4	11.3	5.3	342
	A59	8.12	10.1	0.37	4.57	8.57	122	8.08	21.1	0.78	11.3	19.9	9.82	137
	A64	8.21	10.6	0.46	12.8	12.9	110	4.71	12.2	0.43	15.8	30.3	38.4	178
River water	A05	8.84	6.8	0.58	18.8	31.6	223	10.9	37.7	2.87	18.6	41.1	0.58	263
	A07	8.51	4.2	0.42	69.5	441	181	10.1	270	3.3	18	38	1.62	932
	A25	8.69	8	0.68	30.3	51.8	184	10.1	58.9	1.38	19.5	26.5	0.352	281
	A38	8.76	10.3	0.39	7.38	11.3	175	8.41	11.8	1.29	13.1	40.4	1.92	175
	A41	8.81	6.2	1.13	80.6	41.3	365	33.5	134	4.28	43.3	21.9	1.23	509
	A47	8.93	8.8	0.74	10.4	22.1	144	8.62	20.3	1.75	13.5	30.1	1	171

Table 2 (continued)

Types	Samples	pH	Temp ℃	EC	Cl− mg/L	SO42−	HCO3−	CO32−	Na+	K+	Mg2+	Ca2+	NO3−	TDS
River water	A48	9.1	9.1	0.67	33.1	73	149	8.37	42.2	1.36	25	30.3	5.98	285
	A51	8.68	10.8	0.68	28.8	28.2	203	14.8	46.7	1.81	28.3	18.6	0.283	254
	A63	8.76	2.7	0.38	4.73	11.6	111	5.94	11.2	0.55	10.2	24.3	2.07	120

Temp is the abbreviation for temperature, '–' represents samples that were not tested

Table 3 Statistical hydrochemistry and isotope results in the high-water period

Type	Index	pH	EC mS/cm	Cl^- mg/L	SO_4^{2-}	HCO_3^-	Na^+	K^+	Mg^{2+}	Ca^{2+}	NO_3^-	TDS	δD (%)	$\delta^{18}O$
Pore water	Min	7.5	0.4	5	8	182	10	0.8	10	43	0	194	– 80.6	–10.6
	Max	8.6	1.2	104	228	481	152	9.7	40	147	48	674	– 57.7	– 6.9
	Mean	8.0	0.7	25	57	269	32	2.3	17	75	11	354	– 64.0	– 8.0
Pore–fissure water	Min	7.5	0.4	5	8	183	11	0.4	0.7	3	6	210	– 79.8	– 9.8
	Max	9.6	1.1	79	94	351	138	4.4	34	95	95	525	– 60.7	– 6.6
	Mean	8.2	0.6	23	34	238	53	1.1	15	44	33	321	– 68.6	– 8.5
River water	Min	8.0	0.5	8	6	236	19	0.9	12	29	0.3	237	– 64.6	– 8.4
	Max	8.9	1.5	83	287	573	248	5.2	33	70	20	847	– 48.0	– 6.4
	Mean	8.5	0.8	35	59	335	88	2.7	23	46	5	428	– 57.5	– 7.4

negative, whereas two positive indices is indicative of the reverse reaction. The chloro-alkaline indices are defined as following:

$$\mathrm{CAI}-1=\frac{\mathrm{Cl}^- - (\mathrm{Na}^+ + \mathrm{K}^+)}{\mathrm{Cl}^-} \tag{3}$$

$$\mathrm{CAI}-2=\frac{\mathrm{Cl}^- - (\mathrm{Na}^+ + \mathrm{K}^+)}{\mathrm{SO}_4^{2-} + \mathrm{HCO}_3^- + \mathrm{CO}_3^{2-} + \mathrm{NO}_3^-}, \tag{4}$$

where the unit of all ions is meq/L.

The piston model is used to estimate the age of groundwater according to the content of the tritium isotope (^3H) (Zhao et al. 2017):

$$C_{out} = C_{in}(t-\tau)e^{-\lambda\tau}, \tag{5}$$

where C_{out} is the tritium concentration in groundwater, C_{in} is tritium concentration in atmospheric precipitation, t is the time series of tritium output, τ is the retention time of tritium in groundwater, and λ is the tritium decay constant (0.055764).

Results and discussion

Hydrochemical characteristics of groundwater

Statistical summary of the chemical content of groundwater

Chemical constituents in the porous medium aquifer The statistical summary of the results from the analysis of the porous medium aquifer samples in the high-water period listed in Table 3. The pH ranges of groundwater in this aquifer was found to vary from 7.5 to 8.6 with a mean of 8.0, and the average TDS in this aquifer was is 354 mg/L. The mean concentrations of Ca^{2+}, Na^+, and Mg^{2+} were 75, 32, and 17 mg/L, respectively, and the mean concentrations of HCO_3^-, SO_4^{2-}, and Cl^- were 269, 57, and 25 mg/L, respectively (Table 3). According to their mean contents, the order of major ions in the pore-water aquifer (from high to low) are HCO_3^-, SO_4^{2-}, Cl^- for anions and Ca^{2+}, Na^+, Mg^{2+} for cations (Table 3).

The statistical summary of results obtained from the porous medium aquifer in the low-water period are listed in Table 4. During this period, the pH was found to range from 7.6 to 8.6 with a mean of 8.2, and the average TDS is 262 mg/L. The mean concentrations of Ca^{2+}, Na^+, and Mg^{2+} are 48, 29, and 15 mg/L, respectively, and the mean

Table 4 Statistical hydrochemistry and isotope results in the low–water period

Type	Index	pH	ECmS/cm	Cl^- mg/L	SO_4^{2-}	HCO_3^-	Na^+	K^+	Mg^{2+}	Ca^{2+}	NO_3^-	TDS
Pore water	Min	7.6	0.4	5	10	94	10	0.6	1	5	0	165
	Max	8.6	1.2	43	255	221	139	5.8	27	116	64	620
	Mean	8.2	0.6	18	56	171	29	1.7	15	48	10	262
Pore-fissure water	Min	7.4	0.4	4	8	93	12	0.3	0	3	0.6	137
	Max	9.8	1.0	61	94	255	177	2.5	35	79	110	481
	Mean	8.2	0.6	19	32	171	57	0.9	14	26	28	262
River water	Min	8.5	0.4	5	11	111	11	0.6	10	19	0.3	120
	Max	9.1	1.1	81	441	365	270	4.3	43	41	6	932
	Mean	8.8	0.6	32	79	193	70	2.1	21	30	2	332

concentrations of HCO_3^-, SO_4^{2-}, and Cl^- are 171, 56, and 18 mg/L, respectively (Table 4). According to their mean contents, the order of major ions in pore-water aquifer (from high to low) also are HCO_3^-, SO_4^{2-}, Cl^- for anions and Ca^{2+}, Na^+, Mg^{2+} for cations (Table 4). The results indicates that the order of major ions in the porous medium aquifer is maintained throughout the year.

Chemical constituents in the pore-fissure aquifer The statistical summary of the results obtained from the pore-fissure aquifer samples in the high-water period is also listed in Table 3. The pH was found to range from 7.5 to 9.6 with an average of approximately 8.2, and the mean TDS in this aquifer is 321 mg/L. The mean concentrations of Na^+, Ca^{2+}, and Mg^{2+} are 53, 44, and 15 mg/L, respectively, and the mean concentrations of HCO_3^-, SO_4^{2-}, and Cl^- are 238, 34, and 23 mg/L, respectively (Table 3). According to their mean contents in groundwater, the order of major ions in the pore-fissure aquifer (from high to low) is HCO_3^-, SO_4^{2-}, Cl^- for anions and Na^+, Ca^{2+}, Mg^{2+} for cations (Table 3).

The statistical summary of results obtained from the pore-fissure aquifer in the low-water period is also listed in Table 4. The pH was found to range from 7.4 to 9.8 with an average of approximately 8.2, and the mean TDS in the pore-fissure aquifer is 262 mg/L. The mean concentrations of Na^+, Ca^{2+}, and Mg^{2+} are 57, 26, and 14 mg/L, respectively, and the mean concentrations of HCO_3^-, SO_4^{2-}, and Cl^- are 171, 32, and 19 mg/L, respectively (Table 4). The above results indicates that the order of major ions in the pore-fissure aquifer is maintained throughout the year regardless of season.

Hydrochemical facies of groundwater

Hydrochemical facies of groundwater from the porous medium aquifer Piper diagrams have been widely used to classify hydrochemical types of water samples (Li et al. 2015; Qian et al. 2016) (Fig. 4), and in this study, a Piper diagram was plotted using AqQA software (version 2.8). This indicated that the chemical facies in the porous medium aquifer are mainly HCO_3-Ca (50%) and HCO_3-Ca·Mg (19%) during the high-water period (Fig. 4a). Similarly, the chemical facies in the porous medium aquifer are mainly HCO_3-Ca·Mg (44%), HCO_3·SO_4-Ca·Mg (25%) and HCO_3-Ca (19%) during the low-water period (Fig. 4b).

In general, the hydrochemical facies of the porous medium aquifer in the high-water period is very similar to those in the porous medium aquifer in the low-water period. As shown in Fig. 4, the similar hydrogeochemical types in the porous medium aquifer reveals a relatively homogeneous hydrogeochemical process regardless of season. Therefore, distinct hydrochemical zoning was not observed in the porous medium aquifer.

Hydrochemical facies of Sgroundwater from the pore-fissure aquifer The hydrochemical types of groundwater from the pore-fissure aquifer are mainly HCO_3-Ca·Mg (27%), HCO_3-Na (26%), and HCO_3-Ca (19%) during the high-water period (Fig. 4a). Similarly, the hydrochemical types during the low-water period are mainly HCO_3-Ca·Mg (37%) and HCO_3-Na (30%) (Fig. 4b). In general, the hydrochemical types of groundwater from the porous medium aquifer during the high-water period is very similar to those in groundwater from the pore-fissure aquifer during the low-water period.

As shown in Fig. 4, the diverse water quality compositional types that are present in pore-fissure aquifer suggests that there are relative complex hydrogeochemical process taking place in this aquifer. The hydrochemical facies of the pore-fissure aquifer vary consistently along the groundwater flow direction (Fig. 4). On the whole, these types include HCO_3-Ca and HCO_3-Ca·Mg in the recharge and throughflow areas and HCO_3-Na in the discharge area (Fig. 4). In addition, the TDS of the pore-fissure aquifer also gradually increases from the recharge to discharge area.

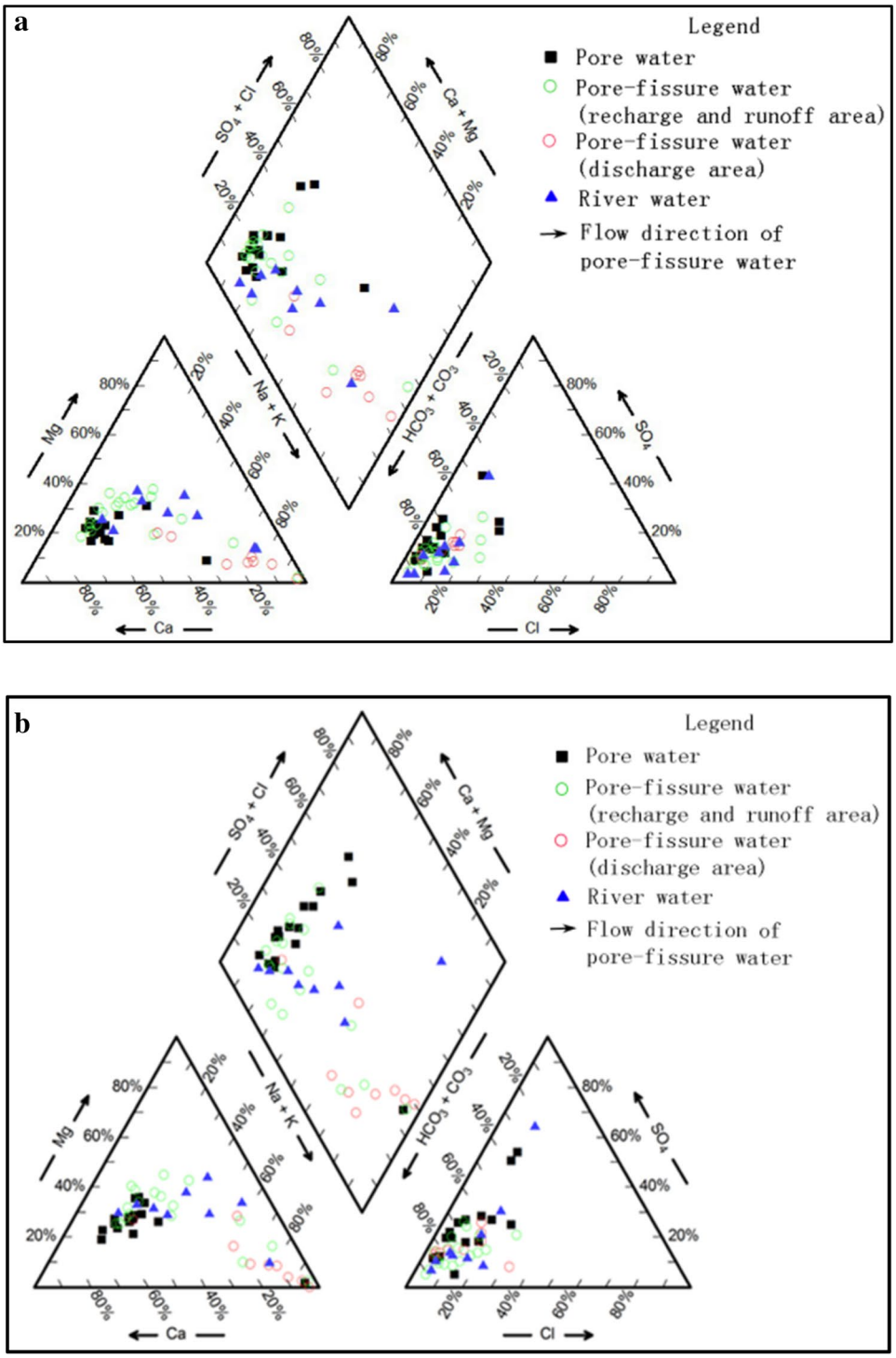

Fig. 4 Piper diagram of groundwater and river water: (**a**) in the high-water period; (**b**) in the low-water period (color figure online)

Similarities and differences between porous medium and pore-fissure aquifers In general, the hydrochemical types of groundwater in both the porous medium and pore-fissure aquifers is similar, as both aquifers have groundwater where HCO_3 is the dominant anion and both have a low TDS. The reasons are as follows. First, the fine sand of Holocene age is widely distributed on the ground surface of study area, which is beneficial to rainfall infiltration because of its good permeability. Second, the capillary height of the fine sand is about 0.5 m, which makes groundwater evaporation difficult (Wang et al. 2002; Hou et al. 2007). Lastly, the similar mineral compositions plays a special role in the hydrochemical facies.

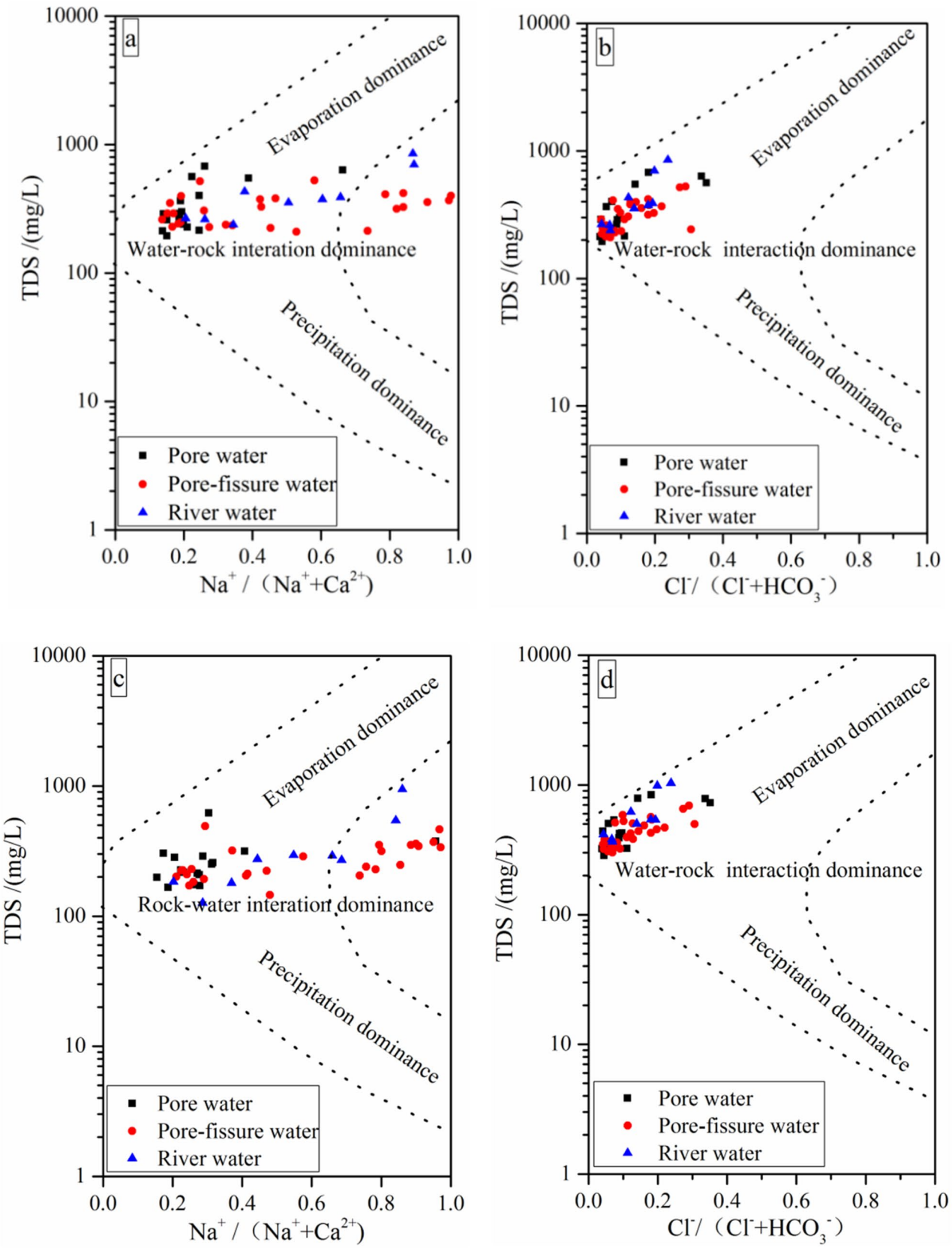
a
Evaporation dominance
Water-rock interation dominance
Precipitation dominance
Pore water
Pore-fissure water
River water
TDS /(mg/L)
Na+ / (Na+ +Ca2+)
b
Evaporation dominance
Water-rock interaction dominance
Precipitation dominance
Pore water
Pore-fissure water
River water
TDS /(mg/L)
Cl- / (Cl- +HCO3-)
c
Evaporation dominance
Rock-water interation dominance
Precipitation dominance
Pore water
Pore-fissure water
River water
TDS /(mg/L)
Na+ / (Na+ +Ca2+)
d
Evaporation dominance
Water-rock interaction dominance
Precipitation dominance
Pore water
Pore-fissure water
River water
TDS /(mg/L)
Cl- / (Cl- +HCO3-)

◂**Fig. 5** Gibbs diagram of groundwater and river water: (**a**) total dissolved solids (TDS) vs. equivalence ratio of $Na^+/(Na^+ + Ca^{2+})$ in the high-water period; (**b**) TDS vs. equivalence ratio ration of $Cl^-/(Cl^- + HCO_3^-)$ in the high-water period; (**c**) total dissolved solids (TDS) vs. equivalence ratio of $Na^+/(Na^+ + Ca^{2+})$ in the low-water period; (**b**) TDS vs. equivalence ratio ration of $Cl^-/(Cl^- + HCO_3^-)$ in the low-water period (color figure online)

The pore-fissure aquifer has a HCO_3-Na composition, whereas the porous medium aquifer does not. The reasons are as follows. Aquifer permeability and seepage path length play a crucial role in the differences observed in hydrochemical facies between two aquifers. The permeability of the porous medium aquifer is substantially higher than that of the pore-fissure aquifer, and the seepage path length is shorter in the porous medium aquifer than in the pore-fissure aquifer. These characteristics influence hydrogeochemical processes.

Processes that influence groundwater hydrogeochemistry

Water–rock interaction

The porous medium and pore-fissure aquifer samples, regardless of season, mainly plot in the water–rock interaction zone of the Gibbs diagram (Fig. 5), which signifies that the major ion contents in groundwater are mostly controlled by mineral dissolution in the aquifer matrix (i.e., calcite and dolomite, feldspar, gypsum).

Application of the Gaillardet diagram further discriminates water–rock interaction types. This diagram suggests that two processes operate in the porous medium aquifer regardless of season: (1) feldspar dissolution and (2) calcite and dolomite dissolution (Fig. 6). The hydrogeochemical processes of the porous medium aquifer broadly correspond with its hydrochemical types.

There are three types that operate in the pore-fissure aquifer regardless of season: (1) and (2) as listed above in the recharge and throughflow area, and (1) and (3) dissolution of a small amount of evaporite minerals (i.e., halite, gypsum) in the discharge area (Fig. 7). The hydrogeochemical processes in groundwater in the pore-fissure aquifer also correspond with its hydrochemical types.

The molar ratio of $(Ca^{2+} + Mg^{2+})/HCO_3^-$ in the porous medium aquifer about 0.5 regardless of season (Figs. 7a, 8a). The molar ratio of Ca^{2+}/HCO_3^- is between 0.25 and 0.5 in this aquifer (Figs. 7b, 8b), and the molar ratio of Ca^{2+}/SO_4^{2-} is greater than 1 (Figs. 7c, 8c). These results indicate that Ca^{2+} is probably mostly derived from the dissolution of calcite and dolomite in the porous medium aquifer with possibly a contribution from the dissolution of gypsum (Qian et al. 2016; Li et al. 2013a; An and Lu 2018).

The molar ratio of $(Ca^{2+} + Mg^{2+})/HCO_3^-$ in recharge and throughflow areas of the pore-fissure aquifer is about 0.5 in regardless of season (Figs. 7a, 8a). The molar ratio of Ca^{2+}/HCO_3^- in this aquifer is between 0.25 and 0.5 (Figs. 7b, 8b), and the molar ratio of Ca^{2+}/SO_4^{2-} is greater than 1 (Figs. 7c, 8c). These imply that the sources of Ca^{2+} in the recharge and throughflow areas of pore-fissure aquifer is the same as the porous medium aquifer. However, groundwater from the pore-fissure aquifer in the discharge area shows molar ratios of $(Ca^{2+} + Mg^{2+})/HCO_3^-$ of less than 0.5 and Ca^{2+}/HCO_3^- is less than 0.25 regardless of season, which are probably related to the effects of feldspar dissolution and cation exchange (An and Lu 2018).

The molar ratio of Na^+/Cl^- in groundwater, both in the porous medium and pore-fissure aquifers, is mostly greater than 1.0 with a low TDS regardless of season (Figs. 7d, 8d). This implies that Na^+ is mainly derived from feldspar dissolution and cation exchange owing to low halite contents (Jalali et al. 2006; Marghade et al. 2012; Li et al. 2013a). Meanwhile, it indicates that the source of Na^+ is not mainly derived from the rainfall.

The gypsum and halite in the groundwater are largely unsaturated regardless of season (Figs. 9a, b, 10a, b), which may indicative the dissolution of these minerals. This hypothesis is further supported by the strong positive correlation between *SI* and concentrations of the relative ions. In light of the hydrochemical characteristics and diagram results, gypsum dissolution is likely a relatively important processes in the groundwater, especially the groundwater from the pore-fissure aquifer in the discharge area.

Almost all samples from the porous medium and pore-fissure aquifers are oversaturated with respect to dolomite and calcite and show a precipitation trend regardless of season (Figs. 9c, d, 10c, d). Gypsum dissolution may lead to the precipitation of dolomite and calcite (Li et al. 2013b). This suggests that the dissolution of dolomite and calcite in the vadose zone may also be a source of the Ca^{2+} and Mg^{2+}. Additionally, a correlation was not observed between the *SI* of carbonate minerals and concentrations of the relevant ions because of precipitation.

Cation exchange

In addition to dissolution/precipitation, cation exchange is also likely to be an important hydrogeochemical process that significantly influences the overall hydrochemistry of groundwater in the study area. Sandy mudstone or sandy clay in the aquifers provide favorable conditions for cation

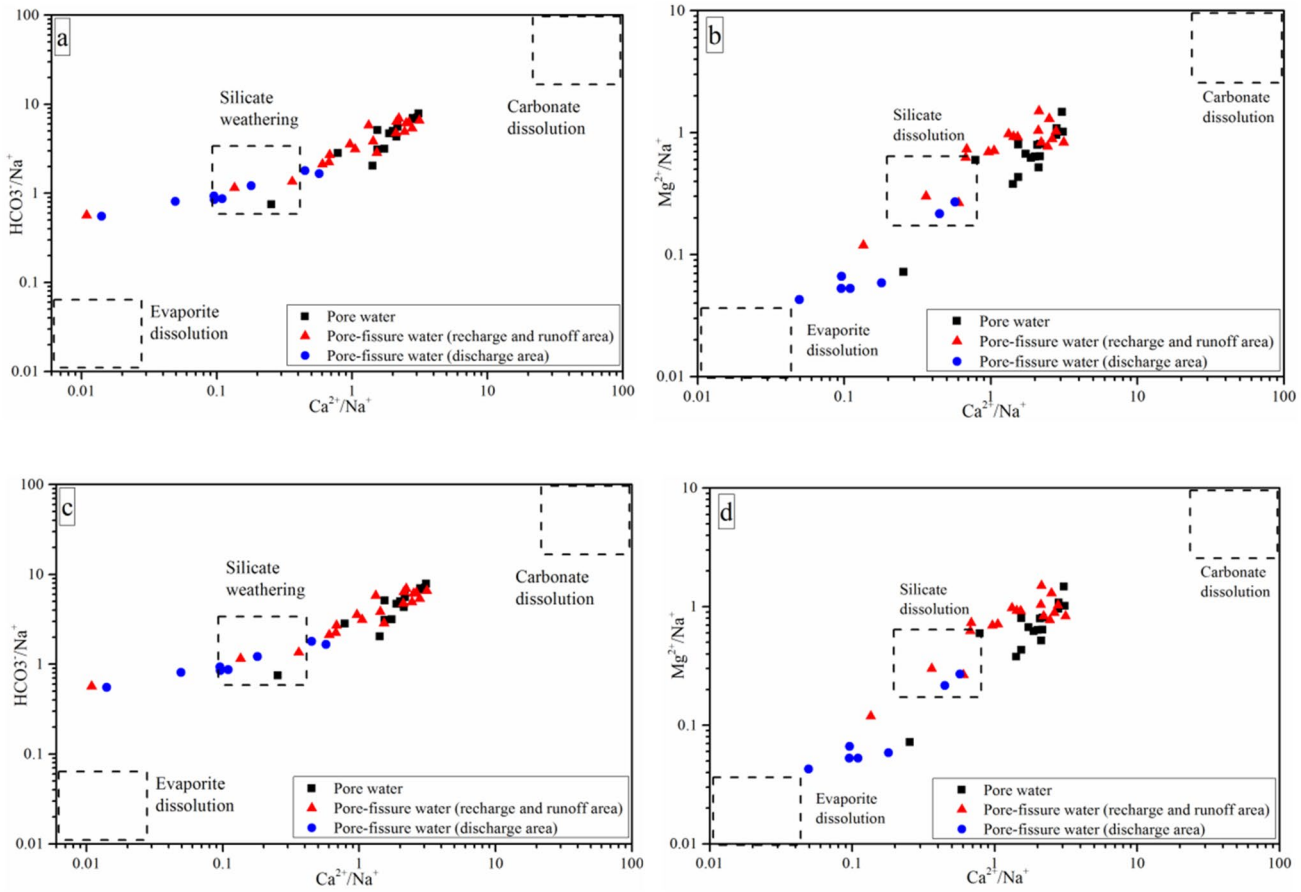

Fig. 6 Gaillardet diagram of groundwater: (**a**) molar ratio of HCO_3^-/Na^+ vs. molar ratio of Ca^{2+}/Na^+ in the high-water period; (**b**) molar ratio of Mg^{2+}/Na^+ vs. molar ratio of Ca^{2+}/Na^+ in the high-water period; (**c**) molar ratio of HCO_3^-/Na^+ vs. molar ratio of Ca^{2+}/Na^+ in the low-water period; (**d**) molar ratio of Mg^{2+}/Na^+ vs. molar ratio of Ca^{2+}/Na^+ in the low-water period (color figure online)

exchange. To explore this possibility, we use chloro-alkaline indices to investigate cation exchange.

Our results indicate that *CAI*-1 and *CAI*-2 values are less than zero in almost all samples regardless of season (Figs. 11a, 12a), which suggests that cation exchange operates widely in groundwater systems in the area and that Ca^{2+} in the groundwater exchanges with Na^+ in the aquifer media. Cation exchange is therefore likely a significant source of Na^+ in the pore medium and pore-fissure aquifers. It is worth mentioning that the extent of cation exchange in the pore-fissure aquifer discharge area is much higher than that in the recharge and throughflow areas.

In addition, diagram showing the relationship between $(Ca^{2+} + Mg^{2+})$-$(SO_4^{2-} + HCO_3^-)$ and $(Na^+ + K^+$-$Cl^-)$ was also used to test for cation exchange (García et al. 2001; Wang et al. 2015; Qian et al. 2016; An and Lu 2018). Cation exchange occurs in the aquifers if the ratio between $(Ca^{2+} + Mg^{2+})$-$(SO_4^{2-} + HCO_3^-)$ and $(Na^+ + K^+$-$Cl^-)$ is about − 1. As shown in Figs. 11b, 12b, most samples plot near the line with a slope of − 1 regardless of season, which also suggests that cation exchange is taking place in the porous medium and pore-fissure aquifers.

Mixing and agricultural activities

A close hydraulic connection exists between the two aquifers in the study area because of good permeability of their sediments and the absence of an extensive aquitard between them (Figs. 2, 3) (Hou et al. 2008a, b). Thus, solutes in groundwater are also exchanged between the two aquifers with groundwater mixing. The similar hydrochemical types between the porous medium and the pore-fissure aquifers further support this point in the study area (Fig. 4).

Elevated concentrations of NO_3^- contents are usually indicative of human activities (Yang et al. 2016; Huang et al. 2018). The NO_3^- concentrations in groundwater in the porous medium aquifer ranged from 0 to 48 mg/L with

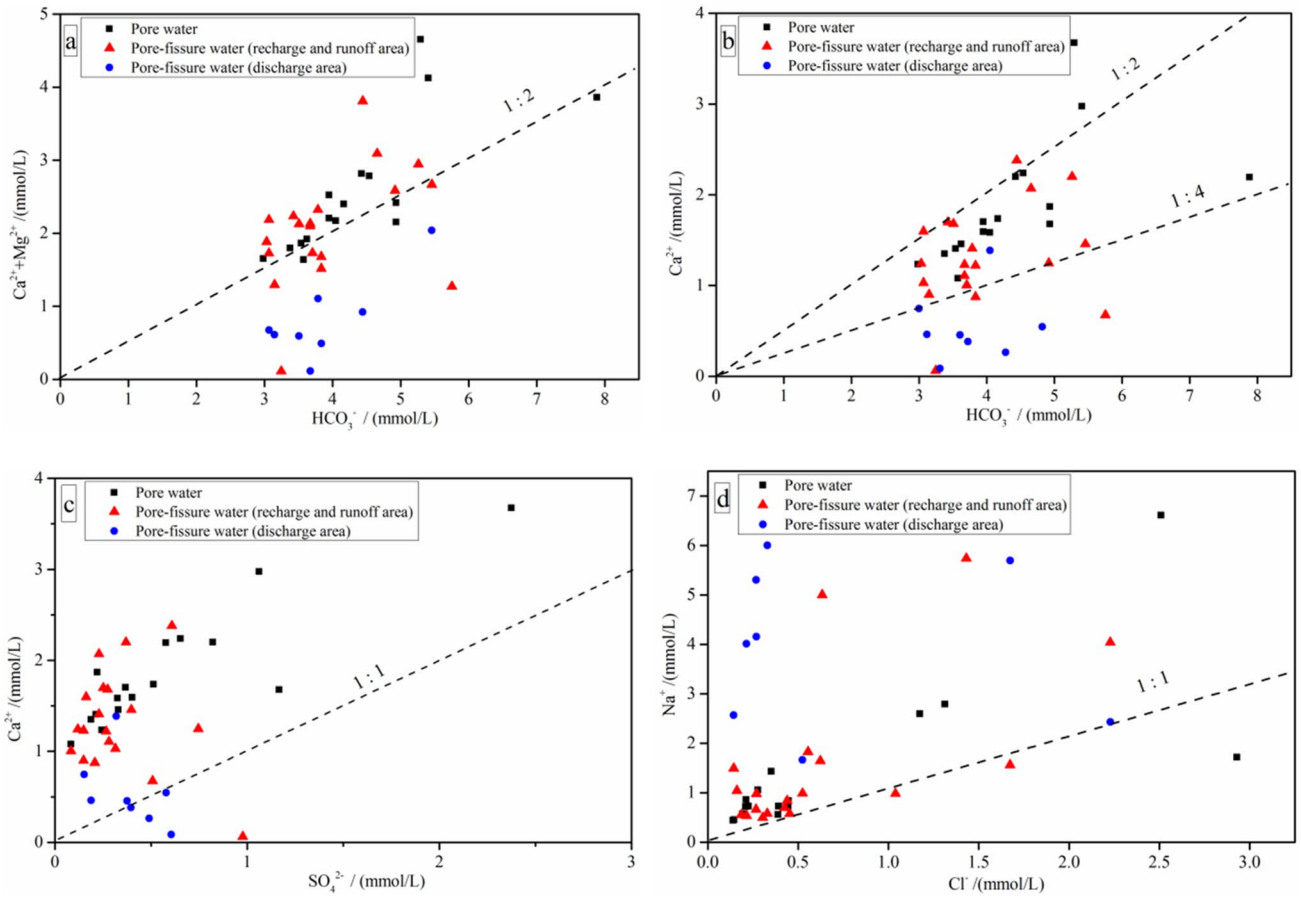

Fig. 7 Ratio diagram of ions in groundwater in the high-water period: (**a**) (Ca^{2+} + Mg^{2+}) vs. HCO_3^-; (**b**) Ca^{2+} vs. HCO_3^-; (**c**) Ca^{2+} vs. SO_4^{2-}; (**d**) Na^+ vs. Cl^- (color figure online)

an average of 11 mg/L during the high-water period, and the NO_3^- concentration in groundwater from the pore-fissure aquifer range from 0 to 64 mg/L with an average of about 10 mg/L during the low-water period (Table 3). Similarly, the NO_3^- in groundwater from the pore-fissure aquifer ranged from 6 to 95 mg/L with an average of 33 mg/L during the high-water period, and the NO_3^- in groundwater in the pore-fissure aquifer ranged from 0.6 to 110 mg/L with an average of about 28 mg/L during the low-water period (Table 4).

It is likely that much of the NO_3^- mainly originates from the use of agricultural fertilizers (Singh 2012; An and Lu 2018; Huang et al. 2018). The fertilizer is likely to seep rapidly into the aquifers with infiltrating rainfall owing to the high permeability of sediments in the vadose zone. The influence of agricultural activities on the hydrochemical composition is, therefore, self-evident, but the effect is only moderate according to the measured NO_3^- concentrations.

Environmental isotopic characteristics

Origin of groundwater

The statistical summary of the environmental isotopes results of the groundwater samples from the high-water period are listed in Table 3. The δD in groundwater form the porous medium aquifer was found to range from − 80.6% to − 57.7% with an average of − 64.0%, and the $\delta^{18}O$ was found to range − 10.6% to − 6.9% with an average of − 8.0% (Table 3). The δD in groundwater form the pore-fissure aquifer was found to range from − 79.8% to − 60.7% with an average of − 68.6%, and the $\delta^{18}O$ levels were found to range − 9.8% to − 6.6% with an average of − 8.5% (Table 3).

The local meteoric water line (LMWL) was established by Hou et al. (2007) in the study area using regression analysis, and is expressed as $\delta D = 6.35\delta^{18}O - 4.69$ (Fig. 13). The slope of LMWL is less than the slope of the global meteoric water line (GMWL, $\delta D = 8\delta^{18}O + 10$) (Crig 1961), which illustrates that atmospheric precipitation is influenced by secondary evaporation under the semiarid climatic

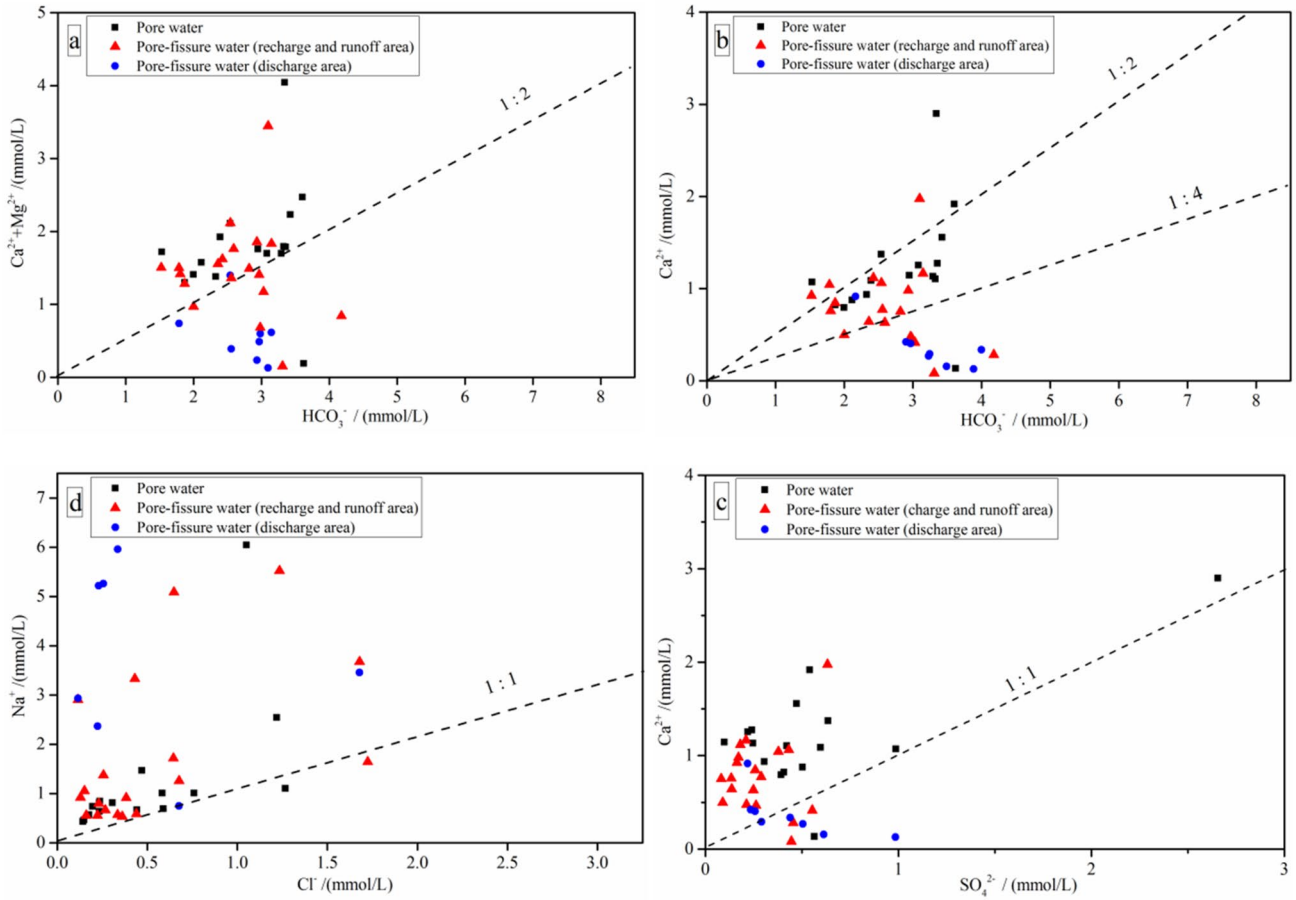

Fig. 8 Ratio diagram of ions in groundwater in the low-water period: (**a**) (Ca^{2+} + Mg^{2+}) vs. HCO_3^-; (**b**) Ca^{2+} vs. HCO_3^-; (**c**) Ca^{2+} vs. SO_4^{2-}; (**d**) Na^+ vs. Cl^- (color figure online)

conditions that occur in the study area (Li et al. 2015; Zhang et al. 2017).

The average $\delta^{18}O$ value is − 8.1% in atmospheric precipitation (Yin et al. 2011b), which is approximately equal to the average values measured in groundwater in the porous medium and pore-fissure aquifers. Similarly, the average δD in atmospheric precipitation is − 58.5% (Yin et al. 2011b), which is approximately the same as the $\delta^{18}O$ average values measured in the porous medium and pore-fissure aquifers (Fig. 13).

Groundwater samples from the porous medium and pore-fissure aquifers plot close to the right side of the LMWL (Fig. 13), which suggests that the origin of groundwater is atmospheric precipitation, as is further supported by the hydrogeochemical process results. This also suggests that some evaporation in the vadose zone occurs during the groundwater infiltration process (Yang et al. 2009). Meanwhile, the stable isotope composition further suggests that evaporation is not a dominant hydrogeochemical processes even though the study area is located in a semiarid region.

Groundwater age and renewability

As shown in Table 1, the concentration of tritium (^3H) in groundwater from the porous medium aquifer was found to range from 10.6 to 20.1 TU with an average of 14.0 TU. In contrast, tritium concentrations below the detection limit (1.3 TU) account for 61.5% of the pore-fissure aquifer groundwater samples, and values of the remaining 38.5% samples range from 2.0 to 5.3 TU with an average of 3.4 TU. The enrichment of tritium is, therefore, a feature of groundwater from the porous medium aquifer, whereas tritium depletion is a feature of groundwater from the pore-fissure aquifer.

To determine the relationship between time and tritium concentrations in the groundwater after 1952, the tritium concentration from the atmospheric precipitation must be determined. Following the method established by Guan (1986), the tritium concentrations between 1956 and 1978 was calculated according to annual rainfall. The tritium concentrations were obtained from 1985 to 1987 and 1995 to 2002 based on data from the IAEA monitoring station (i.e.,

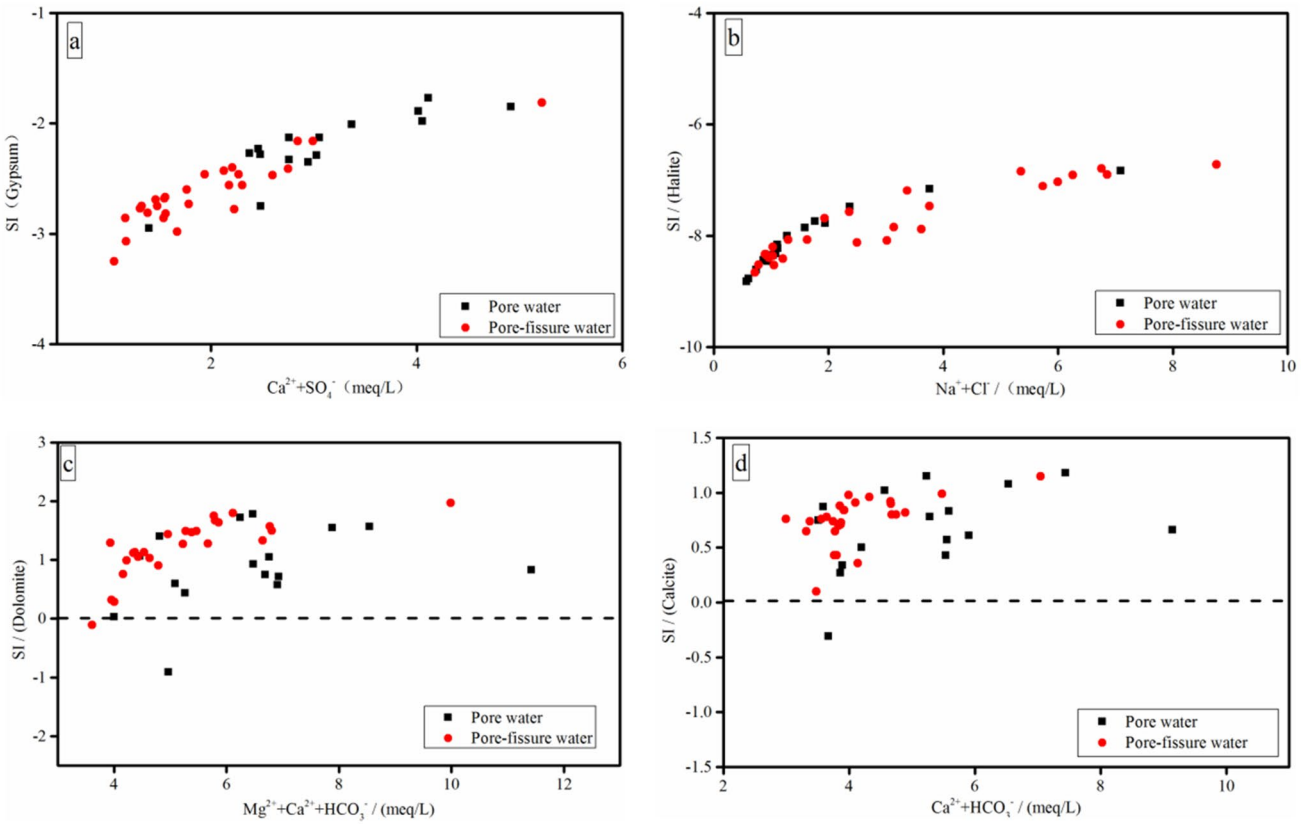

Fig. 9 Relationship diagram of saturation index (*SI*) and relative ions in the high-water period: (**a**) *SI* vs. ($Ca^{2+} + SO_4^{2-}$); (**b**) *SI* vs. ($Na^{+} + Cl^{-}$); (**c**) *SI* vs. ($Mg^{2+} + Ca^{2+} + HCO_3^{-}$); (**d**) *SI* vs. ($Mg^{2+} + Ca^{2+} + HCO_3^{-}$) (color figure online)

Shijiazhuang) around the study area. The triangle interpolation method was used to calculate tritium concentrations between 1988 and 1991 according to IAEA monitoring station data (i.e., Baotou, Yinchuan, Shijiazhuang) around the study area (Zhai et al. 2013). The tritium concentrations in the other time were estimated by the decay law.

Using these methods, the estimated tritium concentration in groundwater in the study area are shown in Fig. 12 as a function of time. The average tritium concentration of groundwater from the porous medium aquifer is estimated to be 14.0 TU, whereas that from the pore-fissure aquifer is estimated to be generally less 5 TU. The average age of groundwater from the porous medium aquifer is approximately 50–60 years (Fig. 14) and it is likely that this aquifer is recharged by modern precipitation. However, the age of the groundwater from pore-fissure aquifer is greater than 50 years (Fig. 14). According to the previous literature (Yang et al. 2004; Hou et al. 2008a, b; Hou et al. 2009), it may range from hundreds to thousands of years and received much of its recharge from precipitation under past climatic conditions. In other words, the age of groundwater from the porous medium aquifer is clearly substantially younger than that from the pore-fissure aquifer. Age has a negative relationship with renewability, which implies that groundwater use from the porous medium aquifer is significantly more sustainable than that from the pore-fissure aquifer.

Aquifer permeability and seepage path length play a crucial role in the differences observed in groundwater renewability between two aquifers. The permeability of the porous medium aquifer is substantially higher than that of the pore-fissure aquifer, and the seepage path length is shorter in the porous medium aquifer than in the pore-fissure aquifer. These characteristics influence groundwater residence times. Therefore, groundwater from the pore-fissure aquifer is depleted in the tritium whereas groundwater in porous medium aquifer is enriched with this isotope.

Relationship between groundwater and river water

The concentration of major ions in the river water is slightly greater than that in the groundwater regardless of season, which may be related to the effects of evaporation from these surface water bodies. The chemical compositions of river water are mainly HCO_3-Ca·Mg and HCO_3-Na·Ca·Mg during the high-water period (Fig. 4a), which are similar to those of the groundwater at the same time of the year. Similarly, the hydrochemical types of river water are mainly HCO_3-Ca·Mg, HCO_3-Ca·Mg·Na and HCO_3-Mg·Na during

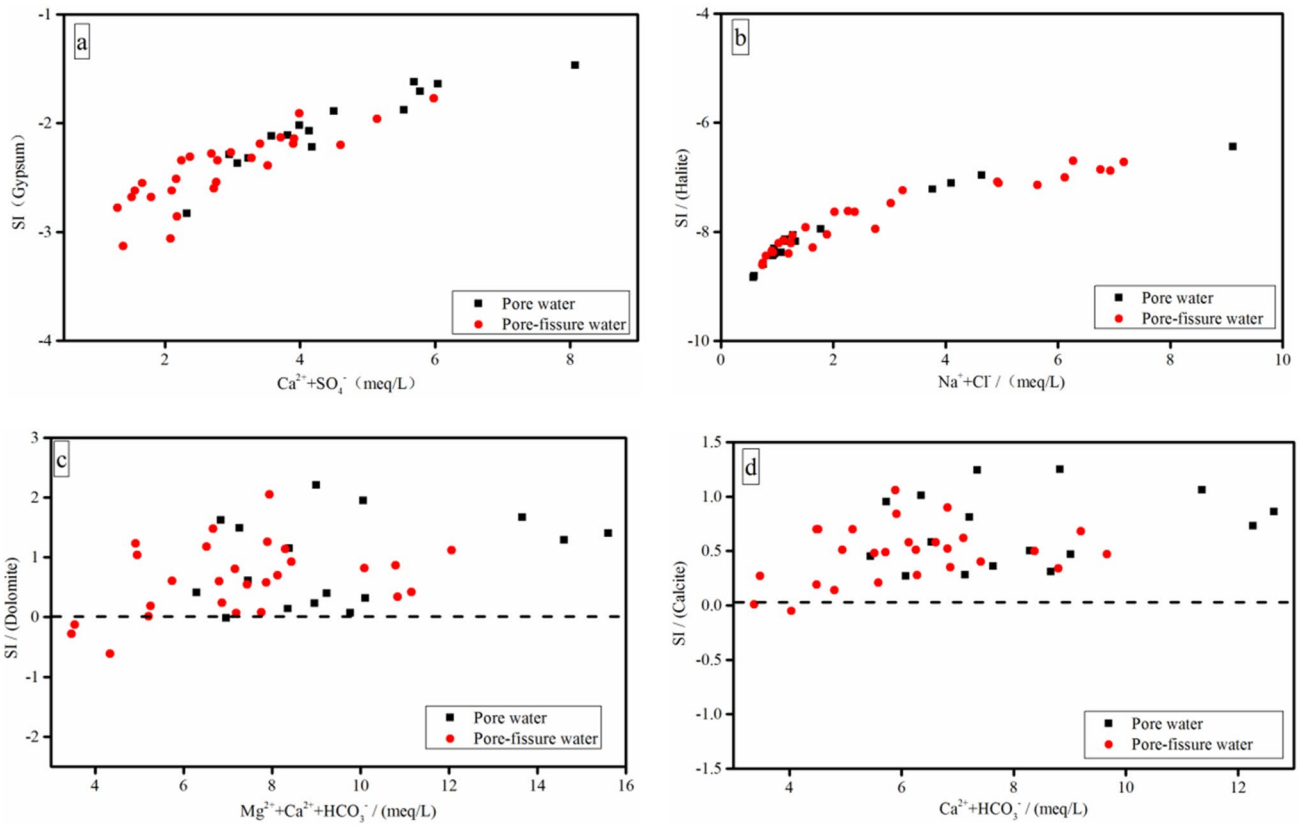

Fig. 10 Relationship diagram of saturation index (*SI*) and relative ions in the low-water period: (**a**) *SI* vs. ($Ca^{2+}+SO_4^{2-}$); (**b**) *SI* vs. ($Na^{+}+Cl^{-}$); (c) *SI* vs. ($Mg^{2+}+Ca^{2+}+HCO_3^{-}$); (d) *SI* vs. ($Mg^{2+}+Ca^{2+}+HCO_3^{-}$) (color figure online)

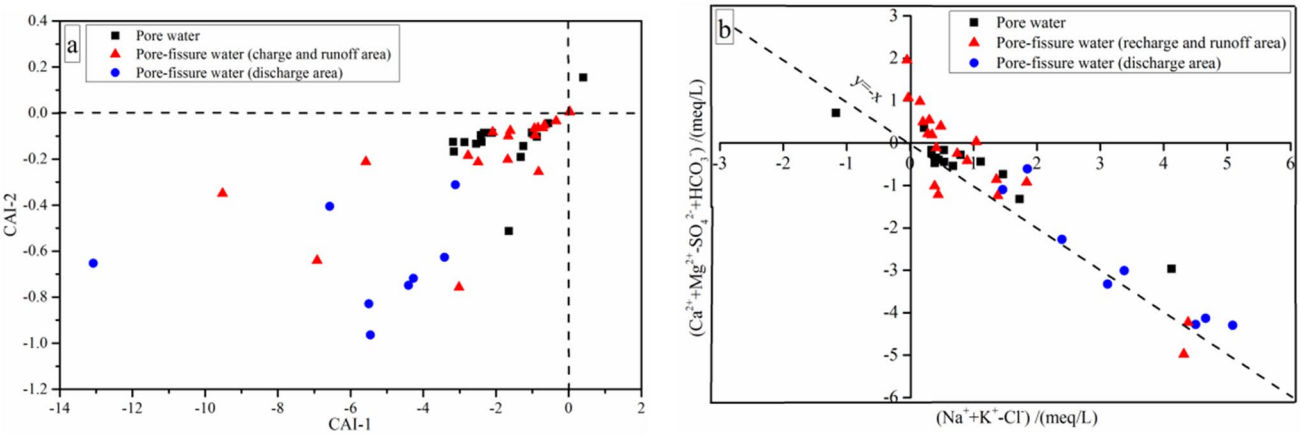

Fig. 11 Diagram of ion exchange: (**a**) chloro-alkaline indices in the high-water period; (**b**) $Ca^{2+}+Mg^{2+}+SO_4^{2-}+HCO_3^{-}$) vs. ($Na^{+}+K^{+}-Cl^{-}$) (color figure online)

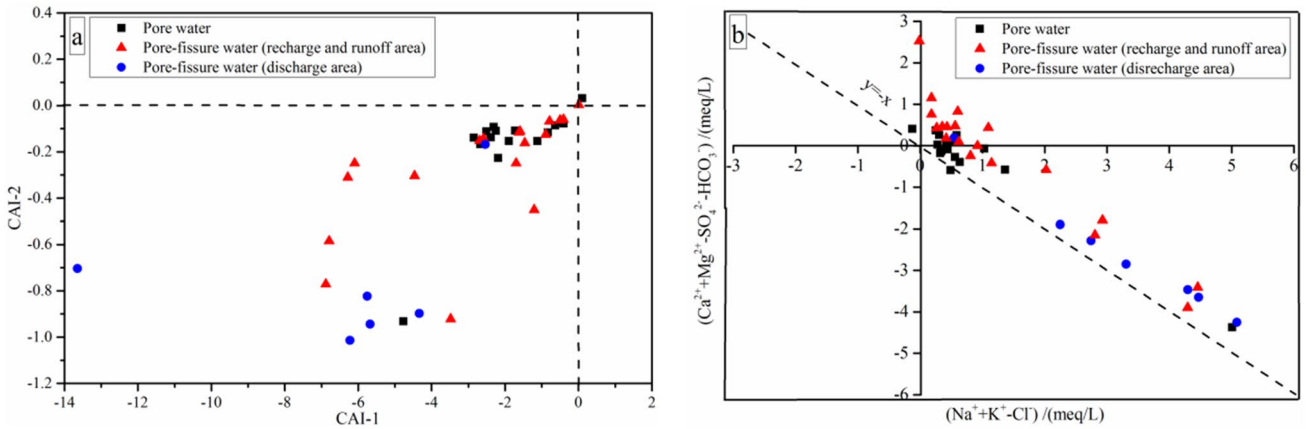

Fig. 12 Diagram of ion exchange in the low-water period: (**a**) chloro-alkaline indices; (**b**) $Ca^{2+} + Mg^{2+} + SO_4^{2-} + HCO_3^-$) vs. ($Na^+ + K^+ - Cl^-$) (color figure online)

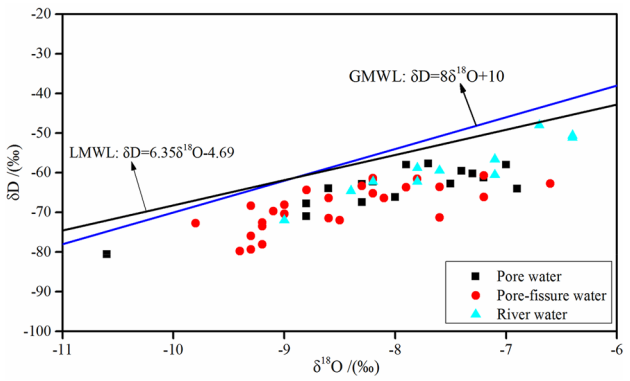

Fig. 13 Relationship diagram between δD and $\delta^{18}O$ in groundwater and river water (color figure online)

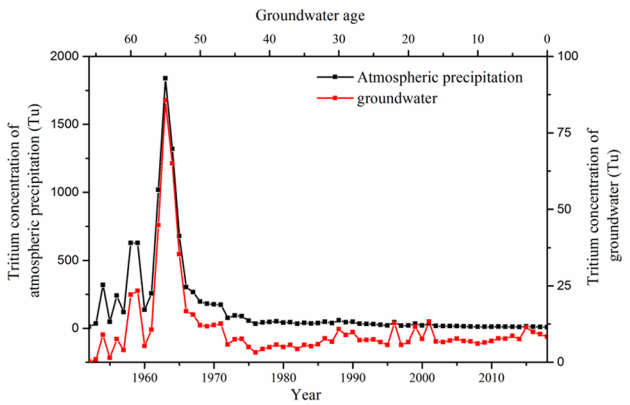

Fig. 14 Curve of tritium concentration in groundwater and atmospheric water as a function of time (color figure online)

the low-water period (Fig. 4b), which are similar to those of the groundwater at the same time of the year. These implies that there is potentially a close hydraulic connection between groundwater and river water in the study area.

The δD in the river water ranges from − 64.6 to − 48.0% with an average of − 57.5%, and the $\delta^{18}O$ ranges from − 8.4% to − 6.4% with an average of − 7.4% in the high-water period. Overall, the composition of D and ^{18}O in the river water is roughly similar to that in groundwater. This also implies that there is likely to be a close hydraulic connection between river water and groundwater.

In general, the river water receives groundwater discharge in the northern part of the Ordos Basin, and amounts for more than 80% of the river flows (Hou et al. 2008a, b; Zhao et al. 2008; Yin et al. 2011b; Feng et al. 2014; Wang et al. 2017a). Because the conditions of landforms and hydrogeology of are similar, it is likely that much of the river baseflow in this area is derived from groundwater discharge. This interpretation is based on three lines of evidences. First, the hydrochemical characteristics of the river water are similar to those of the groundwater regardless of regardless of the time of the year. Second, the river water D and ^{18}O compositions are roughly similar to those in the groundwater. Third, according to field investigations, some springs with low flow rates are found in the river valley because of river cutting.

Conclusions

The Hongjiannao Lake Basin in northwestern China is underlain by two aquifers: a unconsolidated porous medium aquifer, and a pore-fissure aquifer. These aquifers interact with surface water bodies in the watershed and are likely to important for sustain aquatic ecosystems in the area.

The dissolution of feldspar and dolomite and calcite dissolution/precipitation are the primary hydrogeochemical processes that take place in the porous medium aquifer,

followed by cation exchange and gypsum dissolution. The dominant hydrogeochemical processes of the pore-fissure aquifer include the dissolution of feldspars, and dolomite and calcite dissolution/precipitation in the recharge and throughflow areas of the aquifer. Cation exchange and gypsum dissolution are likely to be important processes that influence the composition of groundwater from pore-fissure aquifer in areas where groundwater discharge take place.

In general, the hydrochemical characteristics of groundwater are very similar throughout the year and do not appear to be significantly affected by seasonal changes. The hydrochemical compositions in both aquifers are dominated by HCO_3 as an anion and the groundwater has a low TDS regardless season. The chemical composition of groundwater in the porous medium aquifer is spatially very uniform and does not show a clear zonation pattern along groundwater flow paths. By contract, groundwater in the pore-fissure aquifer varies in the direction of groundwater flow.

Groundwater in the porous medium aquifer is mainly derived from modern precipitation whereas groundwater in the pore-fissure aquifer received recharge from ancient rainfall under a past climate regime. Rainfall that recharges the porous medium aquifer undergoes some evaporation as it infiltrates through the vadose zone due to the semiarid climate regime in the study area. Groundwater from the porous medium aquifer is significantly younger than that from the pore-fissure aquifer. Therefore, the renewability of groundwater from the porous medium aquifer is substantially higher than that from the pore-fissure aquifer.

Baseflow in rivers in the study area is mostly derived from groundwater discharge and water in Hongjiannao Lake is likely to be derived by both groundwater discharge and the inflow of river water. Groundwater, river water, and lake water are in hydraulic connection and each component should be considered in a comprehensive water balance in the study area. The results reported here regarding hydrochemical and environmental isotope characteristics of groundwater provide important information for groundwater resource management and environmental protection in the Hongjiannao Lake Basin.

Acknowledgements The research was financially supported by the National Natural Science Foundation of China (Grant 41972259), the China National Scientific and Technical Support Program (Grant 2018YFC0406404), and the Open Project Program of the Shandong Provincial Lunan Geo-engineering Exploration Institute (Grant LNY2020-Z01). The authors would like to thank the editor and the reviewers for their constructive suggestions.

References

Adams S, Titus R, Pietersen K, Tredoux G, Harris C (2001) Hydrochemical characteristics of aquifers near Sutherland in the Western Karoo, South Africa. J Hydrol 241(1):91–103

An Y, Lu W (2018) Hydrogeochemical processes identification and groundwater pollution causes analysis in the northern Ordos Cretaceous Basin. China Environ Geochem Health 40(4):1209–1219

Cartwright I, Morgenstern U (2012) Constraining groundwater recharge and the rate of geochemical processes using tritium and major ion geochemistry: ovens catchment, Southeast Australia. J Hydrol 475(19):137–149

Craig H (1961) Isotope variation in meteoric waters. Science 133:1702–1703

Deng GS, Xie Y, Xie GH, Wang J, Jiang XS, Li MH, Min JK (2008) Characteristics of Cretaceous aquifer sandstone in the Ordos Basin. Sichuan J Geol 28(2):124–130 (**in Chinese**)

Feng LH, Hu FS, Wan L (2014) Assessment of groundwater resources based on AutoCAD technique. Environl Earth Sci 71(5):2143–2154

Gaillardet J, Dupre B, Allegre CJ, Negrel P (1997) Chemical and physical denudation in the Amazon River Basin. Chem Geol 142:141–173

Gaillardet J, Dupré B, Louvat P, Allegre CJ (1999) Global silicate weathering and CO_2 consumption rates deduced from the chemistry of large rivers. Chem Geol 159:3–30

Garcia GM, Hidalgo MDV, Blesa MA (2001) Geochemistry of groundwater in the alluvial plain of Tucuman province. Argent Hydrogeol J 9(6):597–610

Gibbs RJ (1970) Mechanisms controlling world water chemistry. Science 17:1088–1090

Gribovszki Z, Szilágyi J, Kalicz P (2010) Diurnal fluctuations in shallow groundwater levels and streamflow rates and their interpretation - a review. J Hydrol 385:371–383

Guan BJ (1986) Numerical calculation of tritium concentration in precipitation in China. Hydrogeol Eng Geol 13(4):38–41 (**in Chinese**)

Hou GC, Su XS, Lin XY, Liu FT, Yi SP, Dong WH, Yu FK, Yang YC, Wang D (2007) Environmental isotopic composition of natural water in Cretaceous groundwater basin of Ordos and its Significance in water cycle. J Jilin Univ Geosci 37(2):255–260 (**in Chinese**)

Hou GC, Liang YP, Su XS, Zhao ZH, Tao ZP, Yin LH, Yang YC, Wang XY (2008) Groundwater systems and resources in the Ordos Basin. China Acta Geol Sinica 82(5):1061–1069

Hou GC, Zhang MS, Liu F et al (2008) Groundwater investigation in Ordos basin. Geologic Publishing House, Beijing

Hou GC, Liang YP, Yi LH, Tao ZP, Zhao ZH, Yang YC, Wang XY (2009) Groundwater System and Water Resources Potential in Ordos Basin. Hydrogeol Eng Geol 36(1):18–23 (**in Chinese**)

Hou GC, Yin LH, Xu DD (2017) Hydrogeology of the Ordos Basin, China. J Groundwater Sci Eng 5(2):18–29

Houatmia F, Azouzi R, Charef A, Bédir M (2016) Assessment of groundwater quality for irrigation and drinking purposes and identification of hydrogeochemical mechanisms evolution in Northeastern. Tunisia Environ Earth Sci 75(9):1–17

Hu Y, Liu CK, Lu YH, Liu J, Zheng CM (2014) Application of environmental isotopes in understanding hydrological processes of the Heihe River Basin. Adv Earth Sci 29(10):1158–1166 (**in Chinese**)

Huang XJ, Wang GC, Liang XY, Cui LF, Ma L, Xu QY (2018) Hydrochemical and stable isotope (δD and $\delta^{18}O$) characteristics of groundwater and hydrogeochemical processes in the Ningtiaota Coalfield, Northwest China. Mine Water Environ 37:119–136

Hussein MT (2004) Hydrochemical evaluation of groundwater in the Blue Nile Basin, eastern Sudan, using conventional and multivariate techniques. Hydrogeol J 12(2):144–158

Jalali M (2006) Chemical characteristics of groundwater in parts of mountainous region, Alvand, Hamadan. Iran Environ Geol 51(3):433–446

Jiang XW, Wan L, Wang XS et al (2018) A multi-method study of regional groundwater circulation in the Ordos Plateau. NW China Hydrogeol J 26(5):1657–1668

Katz BG, Coplen TB, Bullen TD, Hal DJ (2010) Use of chemical and isotopic tracers to characterize the interactions between ground water and surface water in Mantled Karst. Ground Water 35(6):1014–1028

Li BS, Dong GR, Gao SY, Ding TH, Shen JY, Shao YJ (1991) The change in climatic environment of the Salawusu River Area since the terminal stage of mid-pleistocene as indicated by detrital minerals in quaternary sediments. Acta Petrol Mmineral 10(1):84–90 (**in Chinese**)

Li YF, Wan WF, Wu YG, Hou GC (2006) Application of hydrochemical signatures to delineating portable groundwater resources in Ordos Basin. China Environ Geol 49(3):430–436

Li PY, Qian H, Wu JH, Zhang YQ, Zhang HB (2013) Major ion chemistry of shallow groundwater in the Dongsheng Coalfield, Ordos Basin. China Mine Water Environ 32(3):195–206

Li PY, Wu JH, Qian H (2013) Assessment of groundwater quality for irrigation purposes and identification of hydrogeochemical evolution mechanisms in Pengyang County. China Environ Earth Sci 69(7):2211–2225

Li Y, Hu FS, Xue ZQ, Yu YQ, Wu P (2015) Hydrogeochemical and isotopic characteristics of groundwater in the salt chemical industrial base of Guyuan City Northwestern China Arabian. J Geosci 8(6):3427–3440

Liu F, Song XF, Yang LH, Zhang YH, Han DM, Ma Y, Bu HM (2015) Identifying the origin and geochemical evolution of groundwater using hydrochemistry and stable isotopes in Subei Lake Basin, Ordos energy base, Northwestern China. Hydrol Earth Syst Sci 19(1):551–565

Marghade D, Malpe DB, Zade AB (2012) Major ion chemistry of shallow groundwater of a fast growing city of Central India. Environ Monit Assess 184(4):2405–2418

Qian C, Wu X, Mu WP, Fu RZ, Zhu G, Wang ZR, Wang DD (2016) Hydrogeochemical characterization and suitability assessment of groundwater in an agro-pastoral area, Ordos Basin. NW China Environ Earth Sci 75(20):1–16

Qin DJ, Qian YP, Han LF, Wang ZM, Li C, Zhao ZF (2011) Assessing impact of irrigation water on groundwater recharge and quality in arid environment using CFCs, tritium and stable isotopes, in the Zhangye Basin, Northwest China. J Hydrol 405(1–2):194–208

Singh AK, Mondal GC, Singh TB, Singh S, Tewary BK, Sinha A (2012) Hydrogeochemical processes and quality assessment of groundwater in Dumka and Jamtara districts, Jharkhand. India Environ Earth Sci 67(8):2175–2191

Su XS, Wan YY, Dong WH, Hou GC (2009) Hydraulic relationship between Malianhe River and groundwater: hydrogeochemical and isotopic evidences. J Jilin Univ (Earth Science Edition) 39(6):1087–1094 (**in Chinese**)

Su XS, Cui G, Du SH, Yuan WZ, Wang H (2016) Using multiple environmental methods to estimate groundwater discharge into an arid lake (Dakebo Lake, Inner Mongolia, China). Hydrogeol J 24(7):1–16

Taylor R, Scanlon B, Döll P et al (2012) Ground water and climate change. Nature Climate Change 3:322–329

Wang DQ, Fang L, Hou GC, Ma SJ (2002) Groundwater exploration in the Ordos basin. Northwestern Geol 35(4):167–173 (**in Chinese**)

Wang H, Jiang XW, Wan L, Han GL, Guo HM (2015) Hydrogeochemical characterization of groundwater flow systems in the discharge area of a river basin. J Hydrol 527:433–441

Wang LH, Dong YH, Xu ZF, Qiao XJ (2017) Hydrochemical and isotopic characteristics of groundwater in the northeastern Tennger Desert, Northern China. Hydrogeol J 25:2363–2375

Wang T, Chen J, Ge J, Zhan LC (2017) Isotopic evidence of allogenic groundwater recharge in the Northern Ordos Basin. J Radioanal Nucl Chem 314(3):1595–1606

Winter TC (1999) Relation of streams, lakes, and wetlands to groundwater flow systems. Hydrogeol J 7:28–45

Wu BY, Peng J, Xiang MX, Fan LM (2018) Research on Salawusu formation aquifer protected by water preserving mining in Yushenfu mining area. J Mining Safety Eng 35(5):112–118 (**in Chinese**)

Xie Y, Wang J, Jiang XS et al (2005) Structure of water bearing media and characteristics of water bearing rocks of the Lower Cretaceous aquifer in the Ordos Basin. Hydrogeol Eng Geol (2):11–19 (**in Chinese**)

Xie Y, Deng GS, Liu JQ, Dong WH, Lu HJ (2012) The effects of sedimentary facies and palaeogeography on the formation and distribution of the deep groundwater of the Cretaceous strata in the Ordos Basin. Sediment Geol Tethyan Geol (in China) 32(3):64–74 (**in Chinese**)

Yang YC, Hou GC, Ma SJ (2004) The age and origin of groundwater in the Ordos basin. Northwestern Geol 37(2):97–100 (**in Chinese**)

Yang YC, Shen ZL, Weng DG, Hou GC, Zhao ZH, Wang D, Pang ZH (2009) Oxygen and hydrogen isotopes of waters in the Ordos Basin, China: implications for recharge of groundwater in the North of Cretaceous Groundwater Basin. Acta Geol Sin 83(1):103–113

Yang QC, Wang LC, Ma HY, Yu K, Martín JD (2016) Hydrochemical characterization and pollution sources identification of groundwater in Salawusu aquifer system of Ordos Basin, China. Environ Pollut 216:340–349

Yang N, Wang GC, Shi ZM, Zhao D, Jiang WJ, Guo L, Liao F, Zhou PP (2018) Application of multiple approaches to investigate the hydrochemistry evolution of groundwater in an Arid Region: Nomhon. Northwestern China Water 10(11):1–18

Yang QC, Mu HK, Wang H, Ye XY, Ma HY, Martin JD (2018) Quantitative evaluation of groundwater recharge and evaporation intensity with stable oxygen and hydrogen isotopes in a semi-arid region. Northwest China Hydrol Proc 32(9):1130–1136

Yin LH, Hou GC, Tao ZP, Li Y (2010) Origin and recharge estimates of groundwater in the Ordos plateau, People's Republic of China. Environ Earth Sci 60(8):1731–1738

Yin LH, Hou GC, Dou Y, Tao ZP (2011) Hydrogeochemical and isotopic study of groundwater in the Habor Lake Basin of the Ordos Plateau. NW China Environ Earth Sci 64(6):1575–1584

Yin LH, Hou GC, Su XS, Wang D, Dong JQ, Hao YH, Wang XY (2011) Isotopes (δD and $\delta^{18}O$) in precipitation, groundwater and surface water in the Ordos Plateau, China: implications with respect to groundwater recharge and circulation. Hydrogeol J 19(2):429–443

Zhai YZ, Wang JS, Guo H, Teng GY (2013) Reconstruction and optimization of tritium time series in precipitation of Beijing, China. Radiocarbon 55(1):67–79

Zhang J, Yin LH, Ma HY, Huang JT, Wang XY (2017) Isotope characters of shallow groundwater and their formation in the Ordos Plateau. Arid Zone Research 34(4):748–754 (**in Chinese**)

Zhao ZH, Wang D, Tao ZP, Li Y (2008) Multi-layer circulation model of groundwater flow systems on the Ordos plateau, China: evidence from water head measurements at different depths of a deep borehole by the Packer system. Geol Bull China 27(8):1131–1137 (**in Chinese**)

Zhao LJ, Ruan YF, Xiao HL, Zhou MX, Cheng GD (2014) Application of radioactive trituium Isotope in studying water cycle of the Heihe River Basin. Quaternary Sci 34(5):959–972

Zhao ZH, Wu JC, Yuan GX, Yu X, Sun Q (2017) Recovery and application of tritium concentration in precipitation in northeast of Tarim Basin. Hydrogeol Eng Geol 44(1):16–22 (**in Chinese**)